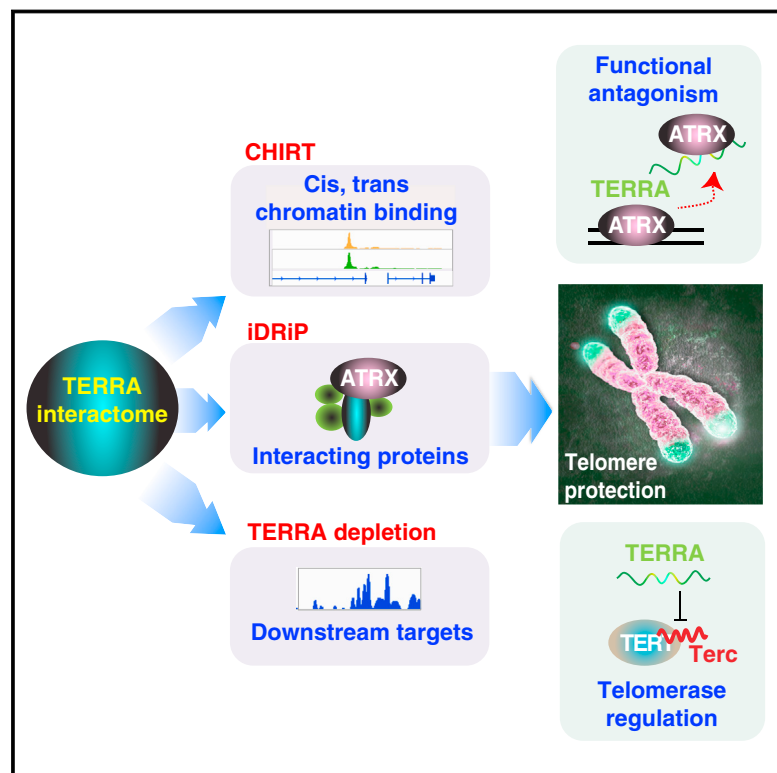


# TERRA RNA Antagonizes ATRX and Protects Telomeres

## Graphical Abstract



## Authors

Hsueh-Ping Chu,  
Catherine Cifuentes-Rojas,  
Barry Kesner, ..., Myriam Boukhali,  
Wilhelm Haas, Jeannie T. Lee

## Correspondence

lee@molbio.mgh.harvard.edu

## In Brief

The functions of the long noncoding RNA TERRA are revealed through a combination of genomic and proteomic approaches, and the helicase ATRX is an important binding partner for its ability to regulate telomere function.

## Highlights

- Epigenomic mapping shows that mouse TERRA RNA binds telomeres and select genes
- iDRiP proteomics reveals that ATRX is a major TERRA-interacting protein
- TERRA and ATRX antagonize each other functionally
- Loss of TERRA results in telomere dysfunction and instability



# TERRA RNA Antagonizes ATRX and Protects Telomeres

Hsueh-Ping Chu,<sup>1,2,3</sup> Catherine Cifuentes-Rojas,<sup>1,2,3</sup> Barry Kesner,<sup>1,2,3</sup> Eric Aeby,<sup>1,2,3</sup> Hun-goo Lee,<sup>1,2,3</sup> Chunyao Wei,<sup>1,2,3</sup> Hyun Jung Oh,<sup>1,2,3</sup> Myriam Boukhali,<sup>4,5</sup> Wilhelm Haas,<sup>4,5</sup> and Jeannie T. Lee<sup>1,2,3,6,\*</sup>

<sup>1</sup>Howard Hughes Medical Institute, Boston, MA 02114, USA

<sup>2</sup>Department of Molecular Biology, Massachusetts General Hospital, Boston, MA 02114, USA

<sup>3</sup>Department of Genetics, Harvard Medical School, Boston, MA 02114, USA

<sup>4</sup>Massachusetts General Hospital Cancer Center, Charlestown, Boston, MA 02114, USA

<sup>5</sup>Department of Medicine, Harvard Medical School, Boston, MA 02114, USA

<sup>6</sup>Lead Contact

\*Correspondence: [lee@molbio.mgh.harvard.edu](mailto:lee@molbio.mgh.harvard.edu)

<http://dx.doi.org/10.1016/j.cell.2017.06.017>

## SUMMARY

Through an integration of genomic and proteomic approaches to advance understanding of long non-coding RNAs, we investigate the function of the telomeric transcript, TERRA. By identifying thousands of TERRA target sites in the mouse genome, we demonstrate that TERRA can bind both *in cis* to telomeres and *in trans* to genic targets. We then define a large network of interacting proteins, including epigenetic factors, telomeric proteins, and the RNA helicase, ATRX. TERRA and ATRX share hundreds of target genes and are functionally antagonistic at these loci: whereas TERRA activates, ATRX represses gene expression. At telomeres, TERRA competes with telomeric DNA for ATRX binding, suppresses ATRX localization, and ensures telomeric stability. Depleting TERRA increases telomerase activity and induces telomeric pathologies, including formation of telomere-induced DNA damage foci and loss or duplication of telomeric sequences. We conclude that TERRA functions as an epigenomic modulator *in trans* and as an essential regulator of telomeres *in cis*.

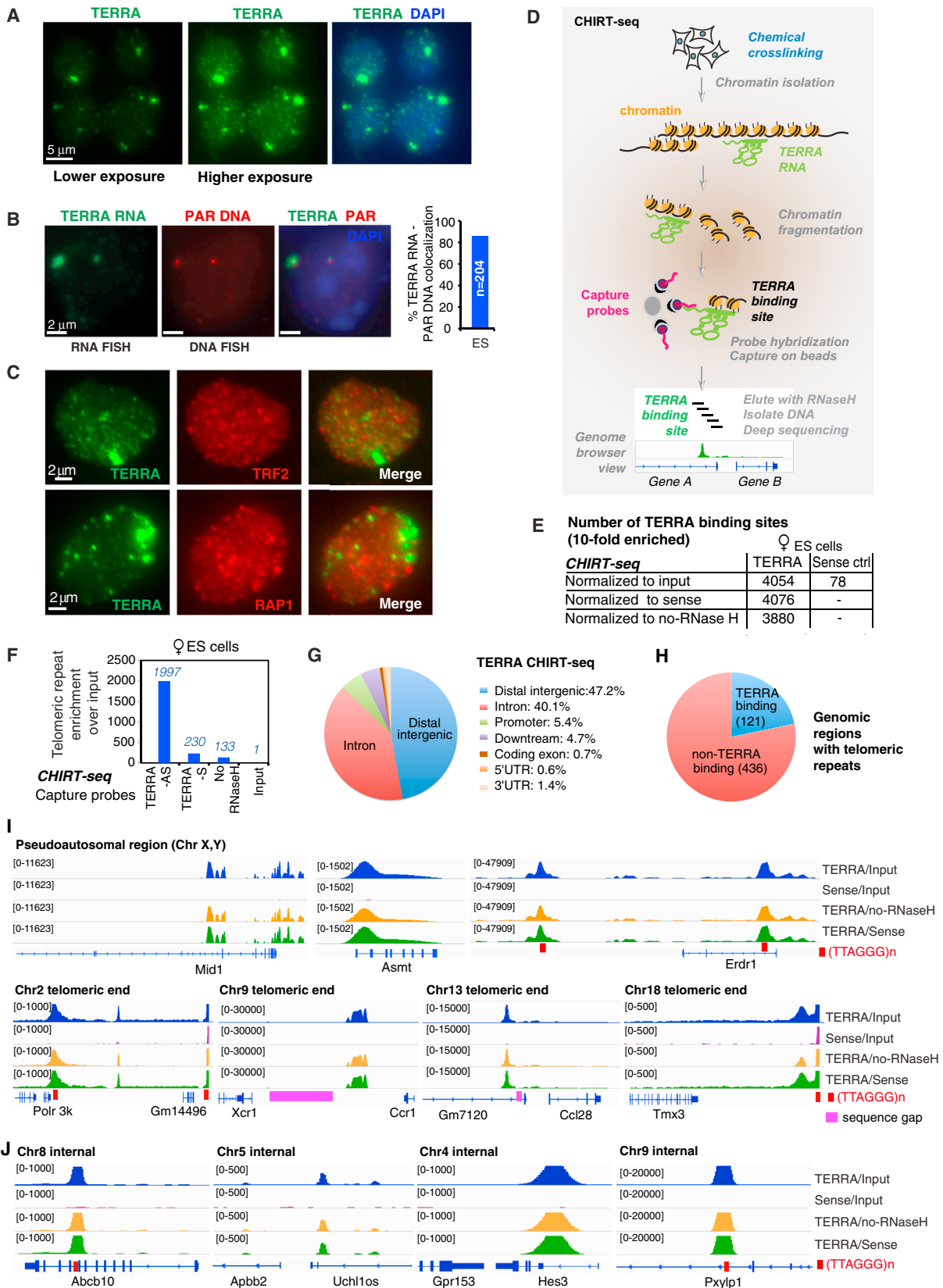
## INTRODUCTION

The Human Genome and ENCODE projects have shown that the protein-coding potential of the mammalian genome is extremely limited (Birney et al., 2007; Kung et al., 2013). Although only 2% of the genome is coding, >90% is transcribed. This transcriptional activity largely produces long noncoding RNAs (lncRNAs), the functions of which have remained mostly unknown. This pervasive transcription extends to the ends of eukaryotic chromosomes. In spite of associated heterochromatin, telomeric ends actively synthesize a heterogeneous population of long noncoding RNAs dubbed TERRA (telomeric repeat-containing RNAs) (Azzalin et al., 2007; Schoeftner and Blasco, 2008; Zhang et al., 2009). TERRA ranges in size from 100 bases to >100 kb

and contains the canonical telomeric repeat sequence, UUAGGG, as well as sequences unique to the subtelomeric region of each chromosome. The function of TERRA has generated major interest in light of its association with human diseases such as cancer, aging, and ICF syndrome (Maicher et al., 2012; Azzalin and Lingner, 2015). Early observations noted that TERRA RNA is localized to the ends of nearly all mammalian chromosomes, with RNA foci being especially prominently associated with sex chromosomes (Azzalin and Lingner, 2008; Schoeftner and Blasco, 2008; Zhang et al., 2009). Cytological studies have also indicated that only about half of detectable TERRA transcripts are localized to telomeres (Le et al., 2013).

Because of the preferential association with telomeres, investigation into TERRA function has focused almost exclusively on telomeres—structures that cap physical ends of linear chromosomes and protect them from unprogrammed shortening and genetic rearrangements (Blackburn et al., 2006; Bernardes de Jesus and Blasco, 2013; Doksanı and de Lange, 2014; Azzalin and Lingner, 2015). Multiple studies have implicated TERRA as regulator of telomerase and telomere length (Sandell et al., 1994; Redon et al., 2010; Maicher et al., 2012; Pfeiffer and Lingner, 2012; Fei et al., 2015). TERRA has also been proposed to regulate recombination between telomeric ends (Balk et al., 2013; López de Silanes et al., 2014; Yu et al., 2014) and serve as a scaffold for recruitment of chromatin factors such as HP1, histone methyltransferases, and shelterins to telomeric heterochromatin (Deng et al., 2009). TERRA therefore appears to be an integral part of telomeric architecture. However, while major progress has been made toward understanding TERRA biology, its specific *in vivo* functions and mechanisms remain ill-defined—especially regarding whether TERRA plays a direct role in each of the proposed functions (Azzalin and Lingner, 2015; Rippe and Luke, 2015).

Major obstacles in the quest to uncover TERRA function have been related to (1) the inability to deplete TERRA RNA by using knockdown technology and the infeasibility of creating TERRA deletions at telomeric ends; (2) an incomplete knowledge of the TERRA protein interactome; and (3) a poor understanding of where TERRA binds in the genome (Maicher et al., 2012; Azzalin and Lingner, 2015; Rippe and Luke, 2015). Similar limitations apply to nearly all lncRNAs, explaining the pervasive



(legend on next page)

challenges associated with studying lncRNA in general. Here, we seek to overcome technical barriers and advance understanding of lncRNAs by combining RNA-centric epigenomics and proteomics approaches. Using TERRA as case study, we generate a map of TERRA's chromatin-interaction sites, define a comprehensive proteome, and establish a method of TERRA depletion to uncover *in vivo* functions. We integrate large datasets with new biochemical and cytological data to identify ATRX as a key interactor and to uncover a major role for TERRA in telomere end protection.

## RESULTS

### TERRA RNA Is Not Restricted to the Telomere

To explore TERRA localization, we performed RNA fluorescence *in situ* hybridization (FISH) with TERRA-specific oligo probes. In low-exposure photographs, one or two prominent TERRA domains were evident in nuclei of 16.7 mouse embryonic stem cells (ESCs) (Figure 1A). Consistent with previous reports (Schoeftner and Blasco, 2008; Zhang et al., 2009), these prominent TERRA foci marked the distal ends of sex chromosomes and colocalized with the pseudoautosomal region (PAR) in >85% of ESCs (Figure 1B). In higher exposure photographs, many additional (albeit smaller) TERRA foci became apparent throughout the nucleus (Figure 1A). TERRA RNA immunoFISH indicated that a subset of pinpoint foci coincided with telomeres, as shown by frequent colocalization with TRF2 and RAP1 (Figure 1C). Interestingly, as only 19.7% of TERRA colocalized with TRF2 (Figure S1A), TERRA may bind non-telomeric sites as well.

For molecular resolution, genomic binding sites for an RNA of interest can be mapped by pulling down associated chromatin with complementary capture probes (Figure 1D). Here, it was necessary to optimize existing methods by combining ChIRP (Chu et al., 2011) and CHART (Simon et al., 2011)—henceforth CHIRT—because TERRA's highly repetitive nature precluded use of tiling probes. The use of a single capture probe (rather than a pool) presented a technical challenge, as (TTAGGG)<sub>n</sub> is present at high copy numbers at all chromosomal ends and capture probes could in principle pull down telomeric DNA rather than the intended TERRA RNA to cause a high background. We optimized various conditions, including use of RNaseH to elute probe(DNA)-RNA interactions, without eluting probe(DNA)-DNA interaction (see STAR Methods for details). We designed two DNA-based capture probes: (1) TERRA anti-

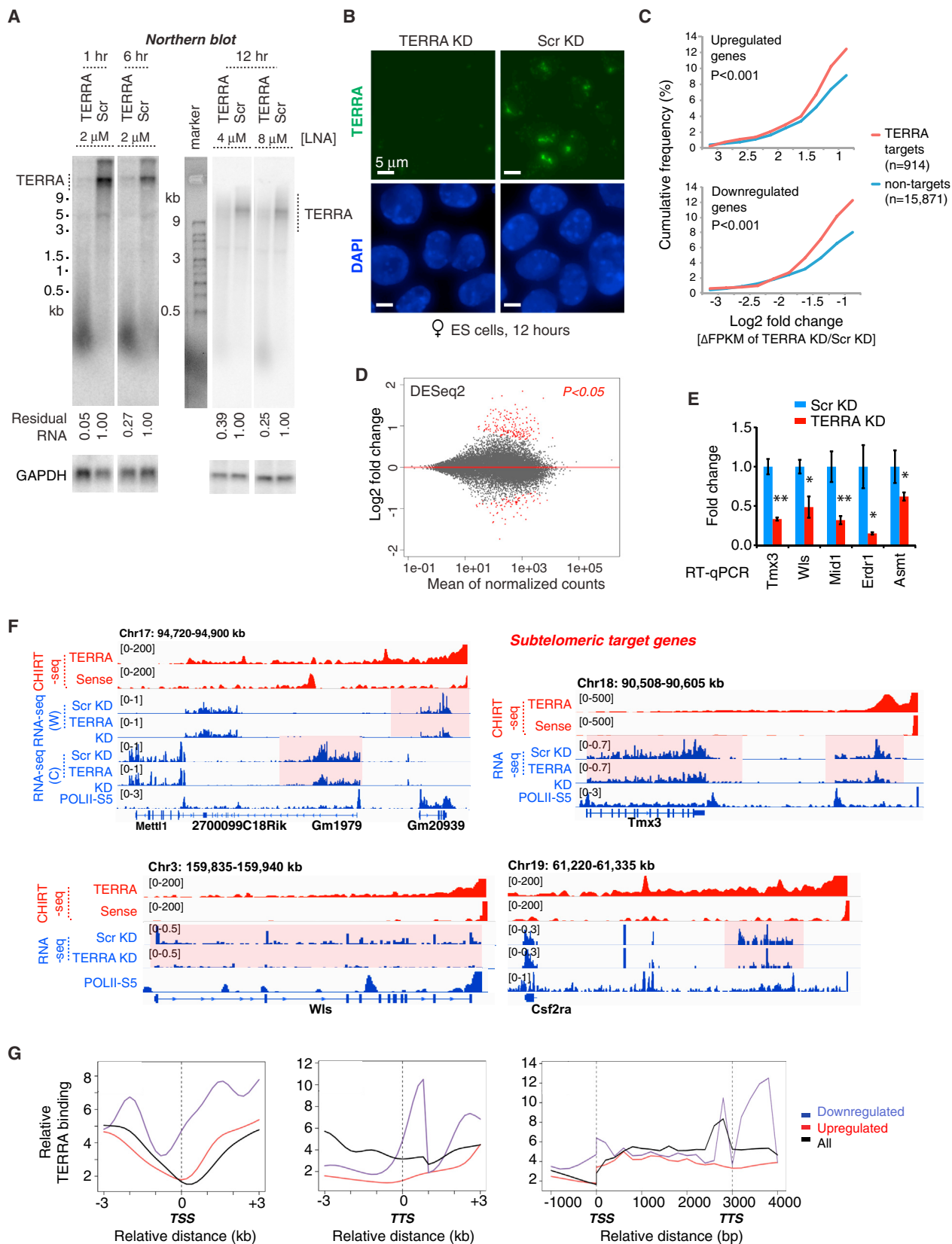
sense (TERRA-AS), to capture transcripts containing UUAGGG repeats, and (2) TERRA sense (TERRA-S, the reverse complement), to control for strand specificity. Slot blot analysis showed that TERRA-AS probes captured TERRA RNA, whereas the corresponding sense probes did not (Figure S1B). Spike-in controls were included for normalization between samples.

To rule out artifacts due to direct probe hybridization to genomic DNA rather than the intended RNA target, we sequenced two controls: (1) an RNaseH– control in which RNaseH was omitted in the elution step, which would in principle preclude elution of RNA-dependent interactions, and (2) a TERRA-S control, which would not hybridize to TERRA RNA but would pull down potential contaminating DNA. Approximately 30 million 50-bp paired-end reads were obtained for each CHIRT library. After removing PCR duplicates, >70% of reads uniquely mapped to the mouse genome. Biological replicates showed a high degree of correlation (Figures S1C and S1D). Regardless of whether we normalized to (1) an input library, (2) a TERRA-S library, or (3) a no-RNaseH library, the results were highly similar (Figure S1E). Using MACS software, we called statistically significant TERRA peaks and identified thousands of binding sites in ESCs (Figure 1E). Whereas ~4,000 binding sites were uncovered when using the TERRA-AS capture probe, <80 were evident when using TERRA-S, suggesting that CHIRT specifically captured TERRA RNA targets.

Major enrichment at telomeric repeat DNA was observed only in the TERRA-AS pull-down and not in TERRA-S or no-RNaseH controls (Figure 1F). The fact that sense and antisense probes yielded dissimilar profiles overall (Figures 1E, 1F, and S1D) argued against hybridization capture of genomic DNA rather than the intended RNA target. Although telomeres were strong binding sites, the vast majority of binding sites actually occurred outside of telomeres (Figures 1G, S1F, and S1G). CEAS (*cis*-regulatory element annotation system) analysis revealed preferential binding to noncoding sequences, with preference for intergenic regions and introns (Figures 1G, S1F, and S1G). Excluding genomic regions containing telomeric repeats did not change the distribution (Figure S1G). The distribution was also similar when CEAS analysis was performed only on genomic regions (internal + telomeric) containing telomeric repeats (Figure S1G). Notably, only a minority (21%) of genomic regions with telomeric repeats were sites of TERRA binding (Figure 1H). Conversely, TERRA-binding sites did not necessarily contain telomeric repeat sequences (Figure S1G). Thus, TERRA binding was not defined by presence of telomeric repeats in the underlying chromatin.

### Figure 1. CHIRT-Seq Analysis Shows that TERRA RNA Binds Chromatin on a Global Scale and Is Not Confined to Telomeres

- (A) RNA FISH shows TERRA foci (green) at low and high exposures in mouse ESCs. DAPI detects nuclear DNA.  
 (B) TERRA prominent spots are associated with the ends of sex chromosomes. TERRA RNA FISH (green) followed by the DNA FISH using the probes (red) derived from the pseudoautosomal regions (PAR) of sex chromosomes. The percentage of TERRA RNA foci colocalized with PAR DNA is shown in the right panel.  
 (C) Partial colocalization of TERRA and telomeres. RNA immunoFISH of TERRA (green) and TRF2 (red, top) or RAP1 (red, bottom). Colocalization counts shown in Figure S1A.  
 (D) Modified CHIRT protocol to capture TERRA binding sites in chromatin.  
 (E) CHIRT results: number of significant TERRA peaks with 10-fold enrichment over background and the length greater than 1 kb in ESCs.  
 (F) TERRA CHIRT-seq showed enrichment for telomeric repeats DNA over input in female ESCs. Samples captured by TERRA-AS or TERRA-S. No-RNaseH for the TERRA-AS capture is also shown as a control. Raw read counts are normalized to spike-in control.  
 (G) CEAS analysis: pie CHIRT shows relative representation of various genomic regions for TERRA binding sites.  
 (H) CEAS analysis: pie chart of genomic regions containing telomeric repeats shows that only ~21% of such regions are bound by TERRA RNA.  
 (I and J) Views of TERRA-binding sites within subtelomeric regions (I) and internal genes (J) of multiple chromosomes.  
 See also Figure S1.



(legend on next page)

Nonetheless, chromosome maps showed greatest TERRA density at or near telomeric ends (Figure S1H; telomeric reads could be unambiguously aligned by their chromosome-specific subtelomeric sequences). TERRA read coverage was high within subtelomeric regions of nearly all chromosomes (chr), most prominently chr 2, 9, 13, 18, and the sex chromosomes, with targets being as much as tens of kilobases away from the telomeric repeat (Figure 1I). Consistent with TERRA RNA FISH, the strongest TERRA binding sites occurred within the pseudoautosomal regions (PARs) of sex chromosomes (Figure 1I). TERRA also bound within internal chromosomal regions and within genes, where it favored introns (Figure 1J). Thus, although TERRA has mainly been studied in the context of telomeres (Le et al., 2013; Rippe and Luke, 2015), TERRA binds chromatin targets throughout the genome. We conclude that TERRA binds both *in cis* at telomeres and *in trans* within or near genes.

### TERRA Depletion Causes Dysregulation of TERRA Target Genes

Determination of TERRA's *in vivo* function requires a method of TERRA depletion. Previous efforts to deplete TERRA RNA (and many other nuclear lncRNAs) have been unsuccessful. Deletional approaches have been infeasible due to the essential nature of telomeric sequences. Knockdown approaches using siRNA and shRNA approaches have also failed to eliminate TERRA. Here, we took an alternative approach and developed single-stranded antisense oligonucleotides (ASOs) with locked nucleic acids (LNA) chemistry and a gapmer design to promote RNaseH-mediated degradation of TERRA RNA *in vivo*. Northern blot analysis showed that treatment of cells with 2  $\mu$ M TERRA-specific ASO resulted in 95% depletion of TERRA transcripts after 1 hr and ~75% depletion after 6 hr (Figure 2A). Longer depletions were more successful with higher concentrations of ASOs (Figure 2A). Regardless of conditions, RNA FISH indicated dramatic effects, as TERRA RNA foci disappeared nearly completely within 1 hr and the depletion lasted for at least 24 hr (Figures 2B and S2A). Thus, gapmer ASOs are an effective means of depleting TERRA.

Transcriptomic analysis at the 12 hr time point showed high reproducibility between two biological replicates (Figure S2B). Cumulative distribution plots (CDPs) demonstrated significant changes in expression of TERRA targets relative to non-targets after TERRA depletion (Figure 2C,  $p < 0.001$ ), indicating that

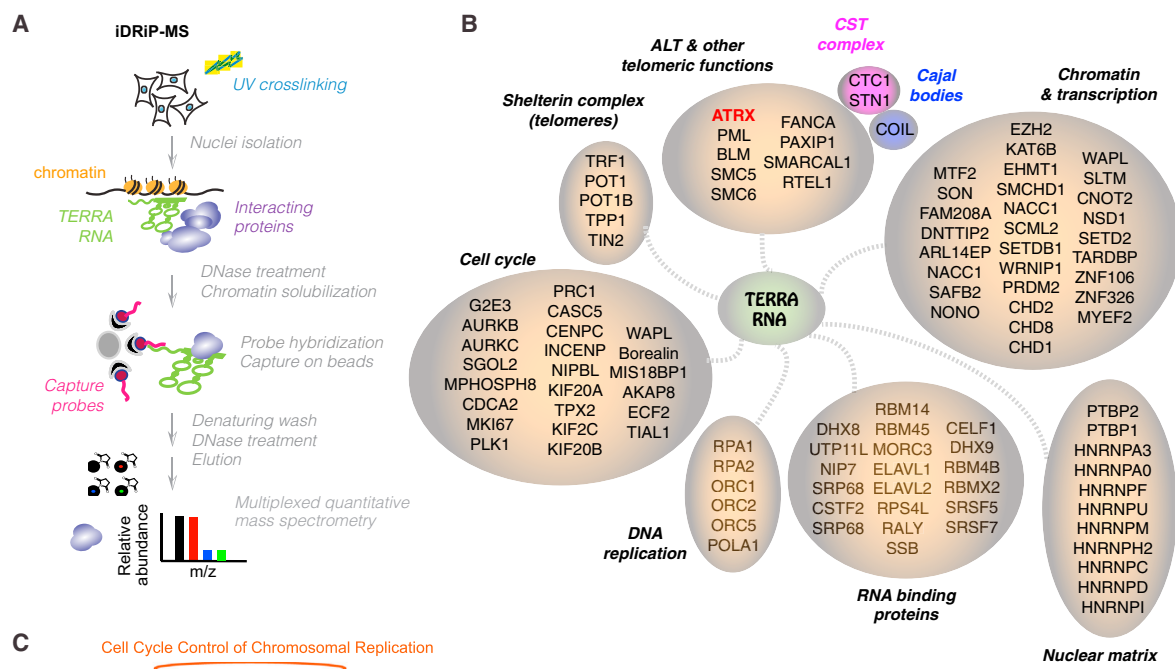
TERRA target genes were more likely to be affected by TERRA depletion. A Bland-Altman M (log ratio) and A (mean average) plot showed significant changes in gene expression after TERRA depletion (Figure 2D and Table S1). Interestingly, subtelomeric target genes were consistently downregulated, as shown by RT-qPCR (Figure 2E) and RNA-seq (Figure 2F; decreased read counts across gene bodies). Internal target genes could either be up- or downregulated (Figures S2C and S2D and Table S1). The sense LNA control yielded a distinct profile with little to no overlap (Figures S2E and S2F), arguing against a nonspecific effect. Gene ontology (GO) analysis indicated that downregulated genes are highly associated with TOR signaling and transcriptional regulation (Figure S3A), whereas upregulated genes are associated with heart development and telomere capping (Figure S3B). There was an intersection of telomerase pathway genes with genes that were upregulated after TERRA depletion (Figure S3C). Intriguingly, metasite and metagene profiles showed greatest TERRA binding densities over genes that were downregulated upon TERRA depletion (Figure 2G). The analysis also revealed a propensity of TERRA RNA to bind genes near the transcription start site (TSS, promoter) and/or the transcription termination site (TTS). This finding was specific to the class of downregulated genes. Upregulated and unaffected genes did not exhibit this propensity. Together, these data demonstrate that TERRA RNA has a direct positive influence on expression of a subset of target genes.

### The TERRA Proteome

To understand how TERRA functions, we next sought to obtain a comprehensive TERRA protein interactome. Proteomic studies to date have largely isolated heterogeneous ribonucleoproteins (hnRNPs) and other general RNA-binding proteins (Ishikawa et al., 1993; López de Silanes et al., 2010; Scheibe et al., 2013; Rippe and Luke, 2015). With one exception (Scheibe et al., 2013), the proteomic analyses have taken *in vitro* approaches. To take an *in vivo* approach, we used iDRiP (identification of direct RNA interacting proteins), which we recently developed to define the Xist proteome (Minajigi et al., 2015). After UV cross-linking of ESCs, TERRA-protein complexes were purified by using TERRA-AS capture probes and washed under denaturing conditions to eliminate proteins that were not crosslinked to TERRA (Figure 3A). Results of a multiplexed quantitative mass spectrometry (Ting et al., 2011; Edwards and Haas, 2016) were

### Figure 2. TERRA Depletion Results in Dysregulation of Gene Expression at Target Sites

- (A) Northern blot analysis of TERRA RNA shows depletion by treatment with gapmer LNA at indicated time points and LNA concentrations in ESCs. Scr, scramble LNA control. GAPDH RNA is used as loading control, and percentage of remaining TERRA RNA is indicated.
- (B) RNA FISH confirming TERRA depletion after 12 hr of LNA treatment. Photos taken with the same exposure.
- (C) Cumulative frequency plots for up- and downregulated genes, showing Log<sub>2</sub> fold changes ( $\Delta$ FPKM) after TERRA KD for the 914 genes with or 15,871 genes without TERRA sites. *p* values determined by 2-tailed Chi-square test with Yate's correction.
- (D) MA Bland-Altman plot to visualize RNA-seq data transformed onto the M (log<sub>2</sub> fold change) and A (mean average) scale. Log<sub>2</sub> fold change represents TERRA KD versus Scr KD. Red dots, genes with significant change ( $P$ -adjust  $< 0.05$ ) using DESeq2 analysis.
- (E) RT-qPCR of subtelomeric genes following TERRA KD. *p* values (\*\*  $< 0.01$ ; \*  $< 0.05$ ) determined by the Student's *t* test. Error bars, SD.
- (F) RNA-seq analysis. Examples of downregulated subtelomeric genes following TERRA KD. All CHIRT data are normalized to input. For all RNA-seq tracks, only the relevant strand is shown, with exception of Chr17 subtelomeric end where both are shown: W, Watson strand; C, Crick strand. RNA-seq coverage was normalized to total mapped fragments.
- (G) Average metasite (left, middle) and metagene (right) profiles for TERRA binding relative to the TSS, TTS, and gene body. Profiles shown for downregulated (blue), upregulated (red), and all (black) genes in TERRA KD.
- See also Figures S2 and S3.



**D**

GO Term	Count	%	P-value	FDR
RNA binding	34	27.6	6.0E-19	8.0E-17
nucleotide binding	52	42.3	7.4E-16	5.2E-14
DNA binding	44	35.8	1.9E-13	8.5E-12
chromatin binding	11	8.9	2.2E-7	7.5E-6
telomeric DNA binding	5	4.1	9.2E-7	2.5E-5
helicase activity	7	5.7	4.0E-4	8.9E-3
ATP binding	23	18.7	7.9E-4	1.5E-2
DNA helicase activity	4	3.3	8.2E-4	1.4E-2
nucleoside binding	24	19.5	9.2E-4	1.4E-2
protein-lysine N-methyltransferase	4	3.3	9.2E-4	1.2E-2

(legend on next page)

then analyzed for enrichment over several negative control samples—those pulled down by TERRA-sense, luciferase (non-mammalian), and U1 (abundant RNA) capture probes (Figure S4).

We averaged two biological replicates and uncovered 134 enriched proteins (>2-fold enrichment compared to luciferase control) belonging to several functional groups (Figure 3B and Table S2): (1) chromatin and transcription factors (e.g., EZH2, SMCHD1), (2) proteins involved in alternative telomere lengthening (ALT), (3) the shelterin complex, (4) cell cycle regulators, (5) DNA replication proteins, and (6) general RNA-binding proteins and nuclear matrix factors. Their absence in the control TERRA-sense iDRiP and their substantial enrichment relative to the luciferase and U1 samples suggested a specific pull-down of TERRA-associated proteins (Figures S4A–S4C). Shelterin proteins, POT1 and TRF1, were ~32-fold enriched over background; telomere-function-associated proteins, PAXIP1 and RTEL1, were >16-fold enriched, as were associated CST complex and Cajal body proteins, CTC1, STN1, and COIL; and ALT-pathway-related proteins, ATRX, PML, and SMC6, were >4-fold enriched (Figure S4C). All noted proteins were significantly enriched over the TERRA-sense pull-down, suggesting a direct association with TERRA RNA rather than telomeric repeat DNA. A subset of the iDRiP-identified factors had previously been shown to bind the telomere (e.g., shelterins and ALT proteins), but the relationship to TERRA RNA was not known (de Lange, 2009; Déjardin and Kingston, 2009; Deng et al., 2009; Grolimund et al., 2013). Thus, in addition to revealing known TERRA interactors, TRF1, POT1 (Deng et al., 2009), nuclear matrix factors, and general RNA-binding proteins (Ishikawa et al., 1993; López de Silanes et al., 2010; Scheibe et al., 2013; Rippe and Luke, 2015), iDRiP uncovered a wide variety of new TERRA-binding proteins.

To visualize interconnections in the TERRA proteome, we analyzed data from iDRiP-MS biological replicates in the context of protein interaction data deposited in public databases. The resulting connectivity map using the Ingenuity Pathway Analysis (Figure 3C) fortified the deduced groupings, and telomere signaling, DNA repair proteins, and cell cycle and DNA replication factors were identified as interaction hubs among the proteomic network for TERRA. Independent analysis using a GO algorithm also revealed enrichment for factors involved in DNA replication, nucleic acid binding, telomere association, helicase activity, and methyltransferases (Figure 3D). The deduced connectome suggests a key organizational role in chromatin regulation, telomere function, DNA replication, and the cell cycle.

### Co-occupancy of ATRX and TERRA on Chromatin Targets

We asked whether enriched interactors colocalize with TERRA RNA in vivo. We correlated our CHIRT data with ESC ChIP

data (Kagey et al., 2010; Law et al., 2010; Pinter et al., 2012; Sarma et al., 2014; Kung et al., 2015; Minajigi et al., 2015) by comparing coverage densities of various chromatin factors to the TERRA landscape (TERRA binding peak  $x = 0$ ) (Figure 4A). Intriguingly, ATRX density was highly correlated with TERRA binding, showing a stronger colocalization than any other chromatin mark. Because ATRX is known to aid deposition of H3K9me3 at telomeres (Clynes et al., 2015), we examined the H3K9me3 histone mark and found significant enrichment at telomeric heterochromatin. Furthermore, TERRA binding was strongly correlated with H3K27me3, the modification placed by EZH2, the catalytic subunit of Polycomb repressive complex 2 (PRC2), which is known to associate with ATRX (Sarma et al., 2014). On the other hand, TERRA was depleted of activate histone marks, including H3K4me3 and H3K36me3, as well as RNA polymerase II, POL-II-S5. TERRA peaks were also depleted of CTCF and cohesins (SMC1 subunit), two factors associated with telomeric transcription (Deng et al., 2012). However, CTCF and cohesins were often found nearby (Figures 4A and S5A). Proteomic data also showed that the cohesin release factor, WAPL, binds TERRA (Figure 3B). The correlative plots held true when telomere-associated TERRA peaks were excluded from analysis (Figure S5A). The only exception was the loss of the H3K9me3 peak, consistent with H3K9me3 being enriched in telomeric constitutive heterochromatin (rather than at genes).

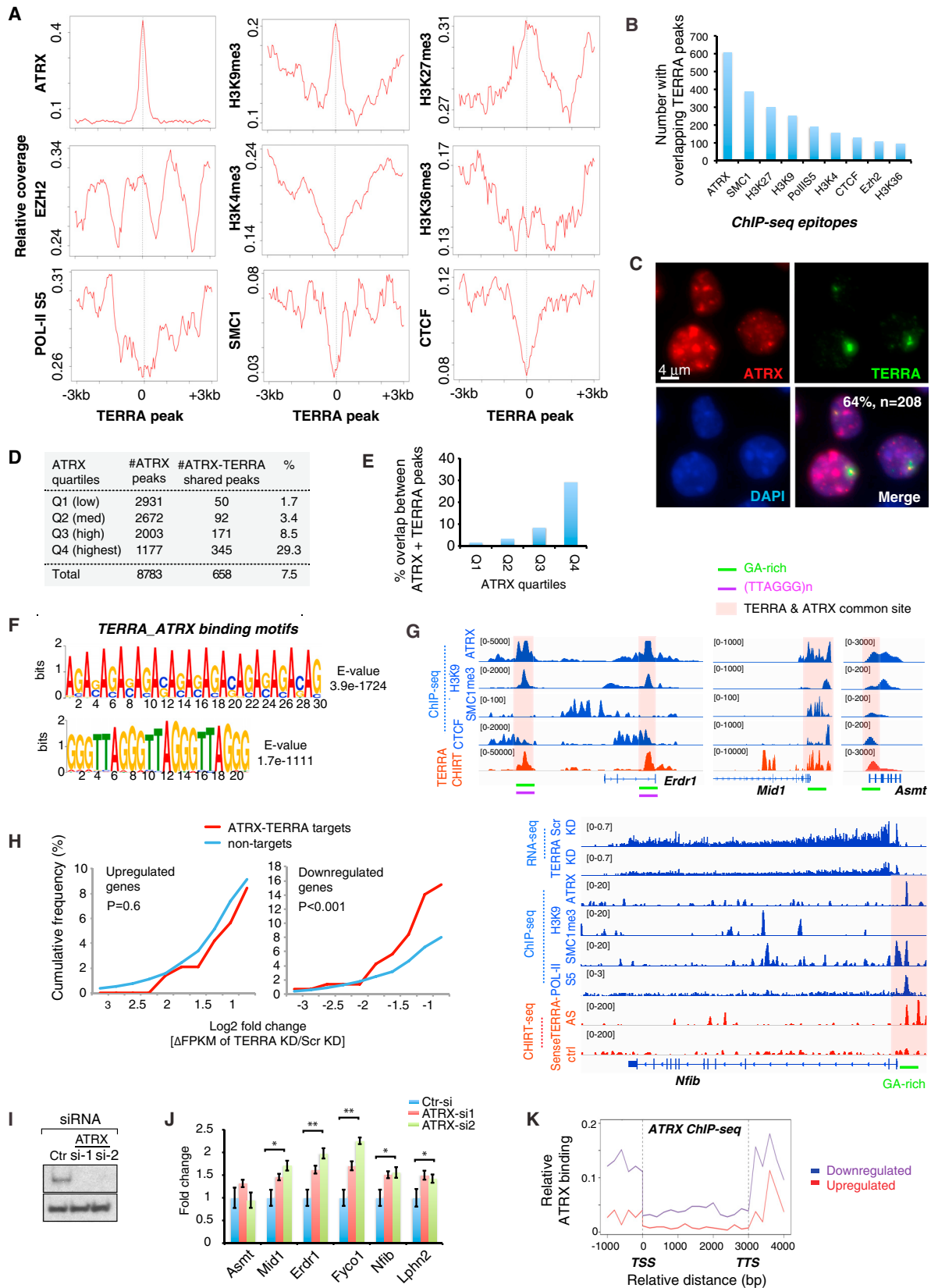
Because ATRX stood out (Figures 4A, 4B, and S5A), we focused analysis on TERRA-ATRX interactions. Immuno-RNA FISH showed that prominent TERRA foci colocalized with a subset of ATRX foci (64%,  $n = 208$ ; Figure 4C). To ask whether TERRA shared a DNA-binding motif with ATRX, we divided ATRX-binding sites into quartiles by coverage densities (low, medium, high, and highest). Intriguingly, ~30% of ATRX sites in the highest quartile (Q4) showed co-occupancy with TERRA RNA (Figures 4D and 4E). The majority of overlapping sites occurred within repetitive sequences. De novo motif analysis using MEME uncovered several common, highly enriched DNA motifs (Figure 4F). The strongest motifs were the (GA) $n$  repeat ( $E$  value =  $3.9e-1,724$ ) and the telomeric repeat including (TTAGGG) $n$  and (CCCTAA) $n$  ( $E$  value =  $1.7e-1,111$ ), examples of which are shown in the colocalized ATRX and TERRA peaks within *Erdr1*, *Mid1*, and *Asmt* (Figure 4G). Thus, TERRA occupies chromatin sites with highest ATRX density and shares binding motifs with its protein partner, ATRX.

### Functional Antagonism between TERRA and ATRX

Given that ATRX is a chromatin remodeler that regulates gene expression (Clynes et al., 2015), we asked whether TERRA modulates gene expression through interaction with ATRX. For the subset of genes targeted by both TERRA and ATRX, there was a significant net downregulation of gene expression after TERRA

### Figure 3. iDRiP-Mass Spectrometry Analysis Reveals an Extensive TERRA Proteome

(A) The iDRiP-MS approach to define the TERRA interactome.  
 (B) TERRA-interacting proteins subclassified into functional groups.  
 (C) Connectivity map for the TERRA interactome using IPA software (QIAGEN). Solid lines, strong direct interactions. Dashed lines, no current evidence for direct interaction. Solid ovals, TERRA interactors. Empty ovals, TERRA non-interactors.  
 (D) GO analysis identified enriched pathways by DAVID bioinformatics resources.  $p$  values determined by Fisher Exact test. Benjamini FDR shown. See also Figure S4.



(legend on next page)

depletion (Figures 4H, S5B, and S5C). At *Nfib*, for example, TERRA RNA and ATRX bound the promoter within a GA-rich motif, and TERRA depletion resulted in reduced expression (Figure 4G), indicating that TERRA binding has a positive influence on *Nfib* expression. Likewise, TERRA depletion resulted in downregulation of the ATRX-TERRA target genes, *Erd1*, *Mid1*, *Asmt*, *Fyco1*, and *Lphn2*, all of which harbor ATRX-TERRA motifs (Figures 4G, 2E, and S5B). These data support a general expression-promoting role for TERRA RNA at TERRA-ATRX target genes. On the other hand, knocking down ATRX protein using two different siRNAs (Figure 4I) resulted in the opposite effect—a significant upregulation of *Mid1*, *Erd1*, *Fyco1*, *Lphn2*, and *Nfib* (Figure 4J). Thus, TERRA and ATRX have opposite effects at shared target genes, with TERRA promoting gene expression and ATRX suppressing it. Supporting this, metagene analysis showed that downregulated genes have significantly higher ATRX binding near the TSS (Figure 4K). This trend was not observed for other epitopes, including H3K4me3 and CTCF (Figure S6). We conclude that, at shared genomic targets, TERRA and ATRX are functionally antagonistic.

#### TERRA Binds ATRX Directly and Antagonizes Localization of ATRX to the Telomere

To determine whether TERRA and ATRX directly interact, we performed electrophoretic mobility shift assays (EMSA) in vitro with purified recombinant ATRX protein and an 83-nt in vitro synthesized TERRA RNA probe. ATRX protein shifted the TERRA transcript (Figure 5A), indicating that the protein directly binds TERRA RNA. It also shifted a 30-nt TERRA RNA probe, but to a lesser degree. By contrast, ATRX did not shift negative controls, U1 splicing RNA (83 nt) and P4P6 ribozyme RNA (156 nt) from *Tetrahymena*. In addition, ATRX's interaction with TERRA RNA could not be competed away by single- or double-stranded DNA (ssDNA, dsDNA) of telomeric repeat sequence (Figures 5B and S7A). On the other hand, TERRA RNA effectively competed away ATRX-DNA complexes (Figure 5C). These data indicate that ATRX forms a more stable complex with TERRA RNA than it does with telomeric DNA. We conclude that TERRA directly and strongly binds ATRX and that this interaction can antagonize ATRX-DNA interactions.

Because TERRA can compete away ATRX-telomeric DNA interactions, we tested whether TERRA may regulate ATRX binding to telomeres in vivo. We combined ATRX immunostaining and telomeric DNA FISH after TERRA depletion for 6 hr in ESCs. Control cells displayed prominent ATRX foci on DAPI-dense pericentric heterochromatin (Figures 5D, 5E, and S7B, asterisks). When depleted of TERRA, cells exhibited dispersed ATRX signals (Figures 5D and 5E). ATRX appeared to relocate to telomeres, as shown by coincident signals with telomeric DNA probes (Figure 5D, arrowheads). The number of ATRX foci found at telomeric DNA significantly increased after TERRA depletion (Figure 5F,  $p < 0.001$ ). These data demonstrate that TERRA plays a role in the localization dynamics of ATRX. Specifically, TERRA antagonizes the binding of ATRX to telomeric DNA. Thus, TERRA regulates ATRX localization to telomeres by competing with telomeric DNA for ATRX binding.

#### TERRA Regulates Telomerase Activity and Maintains Telomere Integrity

Our data collectively hint at specific roles for TERRA in telomere function. Interestingly, RNA-seq and RT-qPCR revealed a 2-fold increase in expression of the telomerase RNA component, *Terc* (Webb and Zakian, 2016), in TERRA-depleted ESCs (Figures 6A and 6B). Because previous in vitro studies had shown that TERRA can bind telomerase reverse transcriptase (TERT) and base pairs with *Terc* telomerase RNA (Redon et al., 2010), we tested whether TERRA can interact with *Terc* in vivo by asking whether *Terc* RNA copurified with TERRA in UV-crosslinked samples. Indeed, we observed enriched pull-down of *Terc* RNA when using TERRA-antisense probes. Enrichment was not seen with TERRA-sense probes or with other negative control probes such as luciferase and U1 (Figure 6C). RNA immunofluorescence (RNA FISH) also showed that 57% of *Terc* foci colocalized with TERRA foci (66/116; Figure 6D). Although we cannot determine whether direct base pairing is involved, these data argue that TERRA occurs in a complex with *Terc* in vivo.

It has also been hypothesized that TERRA regulates telomerase in yeast (Pfeiffer and Lingner, 2012; Moravec et al., 2016). To determine whether TERRA affects telomerase activity in mammalian cells as well, we performed the Telomeric Repeat

#### Figure 4. TERRA and ATRX Target a Common Set of Genes and Are Functionally Antagonistic

- (A) Metasite analysis: ChIP-seq coverage of indicated epitopes (y axis) relative to the averaged genomic TERRA-binding site ( $x = 0$ ).  
 (B) Number of ChIP-seq enriched regions (of indicated epitopes) with an overlapping TERRA peak.  
 (C) Immuno-RNA FISH performed with anti-ATRX antibodies (red) and TERRA-specific probes (green) reveals colocalization of TERRA with a subset of ATRX domains.  
 (D) ATRX chromatin targets in ESCs (ChIP-seq) are divided into four quartiles on the basis of coverage densities (Q4 highest). The number of ATRX peaks and those shared with TERRA are shown, along with the % ATRX peaks shared with TERRA peaks.  
 (E) Percentage of ATRX peaks shared with TERRA is shown for each ATRX quartile.  
 (F) De novo motif analysis using MEME reveals two dominant motifs for TERRA-ATRX target sites. E-values indicate how well each occurrence matches motif.  
 (G) Genome browser shots of TERRA ChIRT-seq and ChIP-seq data for TERRA-ATRX target genes. RNA-seq shows downregulation of *Nfib* after TERRA depletion.  
 (H) TERRA depletion decreases expression of ATRX-TERRA target genes. Cumulative frequency plots of Log<sub>2</sub> fold changes ( $\Delta$ FPKM) for upregulated (Log<sub>2</sub> > 0.75) and downregulated (Log<sub>2</sub> < -0.75) genes after TERRA KD. Profiles for shared ATRX-TERRA targets versus non-targets are graphed. p values determined by two-tailed Chi-square test.  
 (I) Western analysis of ATRX protein after ATRX knockdown (KD) by two gene-specific siRNAs. No protein is detectable after KD.  
 (J) ATRX depletion increases expression of ATRX-TERRA target genes. RT-qPCR assay shows fold changes in expression of indicated genes in ESCs after 48 hr. ATRX siRNA knockdown. Results from several biological replicates. \*\* $p < 0.01$ ; \* $p < 0.05$  two-tailed Student's t test. Error bars, SD.  
 (K) Metagene analysis of ATRX binding. Profiles for genes that are upregulated (red) or downregulated (blue) after TERRA depletion are graphed separately. See also Figures S5 and S6.

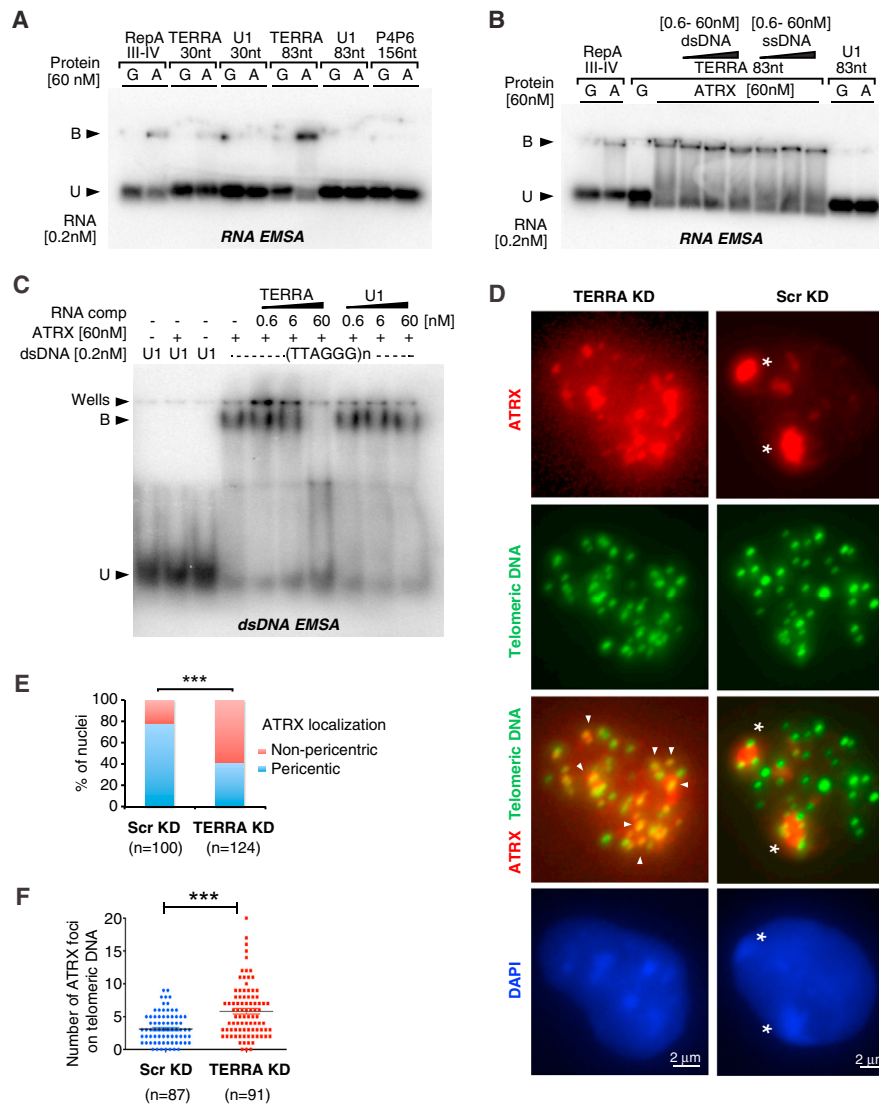


**Figure 5. TERRA Competes with Telomeric DNA for ATRX Binding and Regulates ATRX Distribution**

(A) TERRA binds to ATRX in vitro. RNA EMSA with 0.2 nM RNA probes from indicated transcripts (top) and 60nM GST (G, control) or ATRX (A) protein. Bound probe (shifted), B; unbound, U. RepA derived from Xist RNA as a positive control for ATRX binding. U1 RNA and P4P6 are negative controls.

(B) Competition assay: TERRA RNA shifted by ATRX cannot be competed away by increasing concentrations (0.6, 6, 60 nM) of dsDNA (80 bp) or ssDNA (80 nt) of corresponding TERRA sequence (83 nt). RNA EMSA as described in (A).

(C) TERRA RNA competes away the telomeric dsDNA shifted by ATRX. EMSA with double-stranded U1 or (TTAGGG)<sub>n</sub> telomeric sequence (80bp), in the presence of TERRA or U1 RNA competitor (comp), as indicated.

(D) TERRA depletion (6hr knockdown) causes ATRX dispersal from pericentric heterochromatin and relocation to telomeres in ESCs. Immuno-DNA-FISH staining for ATRX and telomeric DNA reveals large ATRX foci (red) on pericentric heterochromatin (dense DAPI staining) in control cells. TERRA depletion cells show dispersed ATRX signals that coincide with telomeric DNA (green). Asterisks are ATRX foci at pericentric heterochromatin. Arrowheads are ATRX foci at telomeres.

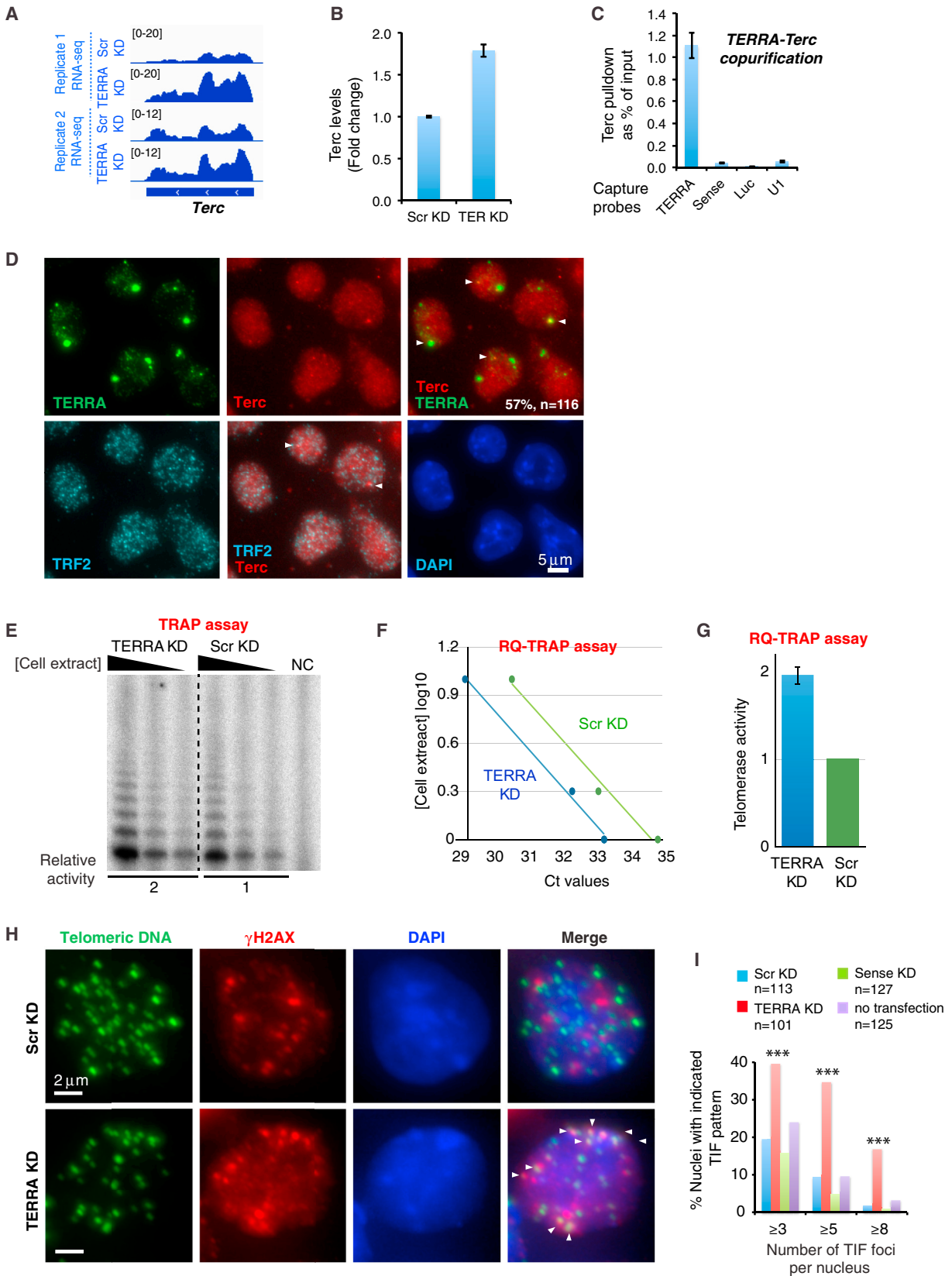
(E) The nucleus with intensive ATRX foci on pericentric chromatin was counted in (D). p value (\*\*<0.001) was determined by Fisher exact test. N, sample size. (F) Dot plot representative of two biological replicates shows the number of ATRX foci on telomeric DNA counted in each nucleus in (D). p value (\*\*< 0.001) was determined by Student's t test. N, sample size.

See also Figure S7.

Amplification Protocol (TRAP) to quantitate telomerase activity in TERRA-depleted ESCs. After 8 hr of TERRA knockdown, we observed a 2-fold upregulation of telomerase activity using both the radio-labeled method (Figure 6E) and the RQ-TRAP

assay (Figures 6F and 6G). Thus, TERRA negatively regulates telomerase activity in vivo.

Given these effects, we surmised that TERRA depletion would cause telomere dysfunction. After treating with TERRA-specific



(legend on next page)

LNAs, we looked for formation of telomere-induced DNA damage foci (TIFs), which typically occur after induction of the DNA damage response at dysfunctional telomeres (Doksani and de Lange, 2014). Significantly,  $\gamma$ H2AX foci accumulated at multiple telomeres in TERRA-depleted ESCs (Figure 6H, arrowheads), consistent with a previous study (Deng et al., 2009). There was a dramatic, significant increase in the number of nuclei with  $\geq 3$ ,  $\geq 5$ , and  $\geq 8$  TIFs (Figure 6I). In Scr and sense LNA controls, TIFs were observed no more frequently than in untransfected cells (Figure 6I). Increased TIF in TERRA-depleted cells suggests a role in maintaining telomeric integrity.

This idea was supported by observed defects in the capping function. With telomere-specific probes, DNA FISH analysis of metaphase spreads revealed loss of telomeric integrity after 24 hr TERRA knockdown, in comparison to knockdown using control scrambled or sense LNA (Figures 7A–7C). Loss of integrity was manifested by significantly increased occurrence of multiple telomeric pathologies (Figures 7A–7D): (1) loss of the (TTAGGG) $_n$  telomeric repeat sequence (arrows) on both sister chromatids or just on one sister chromatid (heterogeneous); (2) duplications of telomeric repeats at chromosomal ends (asterisks); (3) insertions of telomeric repeats within internal chromosomal regions (asterisks); and (4) occasional fusions between sister chromatid telomeres that would create a ring structure (R). Similar results were obtained when DNA FISH was performed with telomeric probes of either strand—C-rich (Figure 7B) versus G-rich (Figure 7C) PNA probes. These pathologies were observed only with TERRA-specific LNA, not with sense LNA, indicating an effect of perturbing TERRA RNA, rather than an effect of LNA binding telomeric DNA. Together, these data point to an essential nature of TERRA in the telomeric capping function and in promoting chromosomal end stability.

## DISCUSSION

Here, we have integrated genomic, proteomic, biochemical, and cytological approaches to advance understanding of TERRA biology. In the mouse ESC genome, we identified thousands of *cis* and *trans* chromatin binding sites and deduced consensus motifs from the binding sites—e.g., (GA) $_n$ , (TTAGGG) $_n$ , and (CCCTAA) $_n$ . Using a TERRA-specific ASO of defined sequence

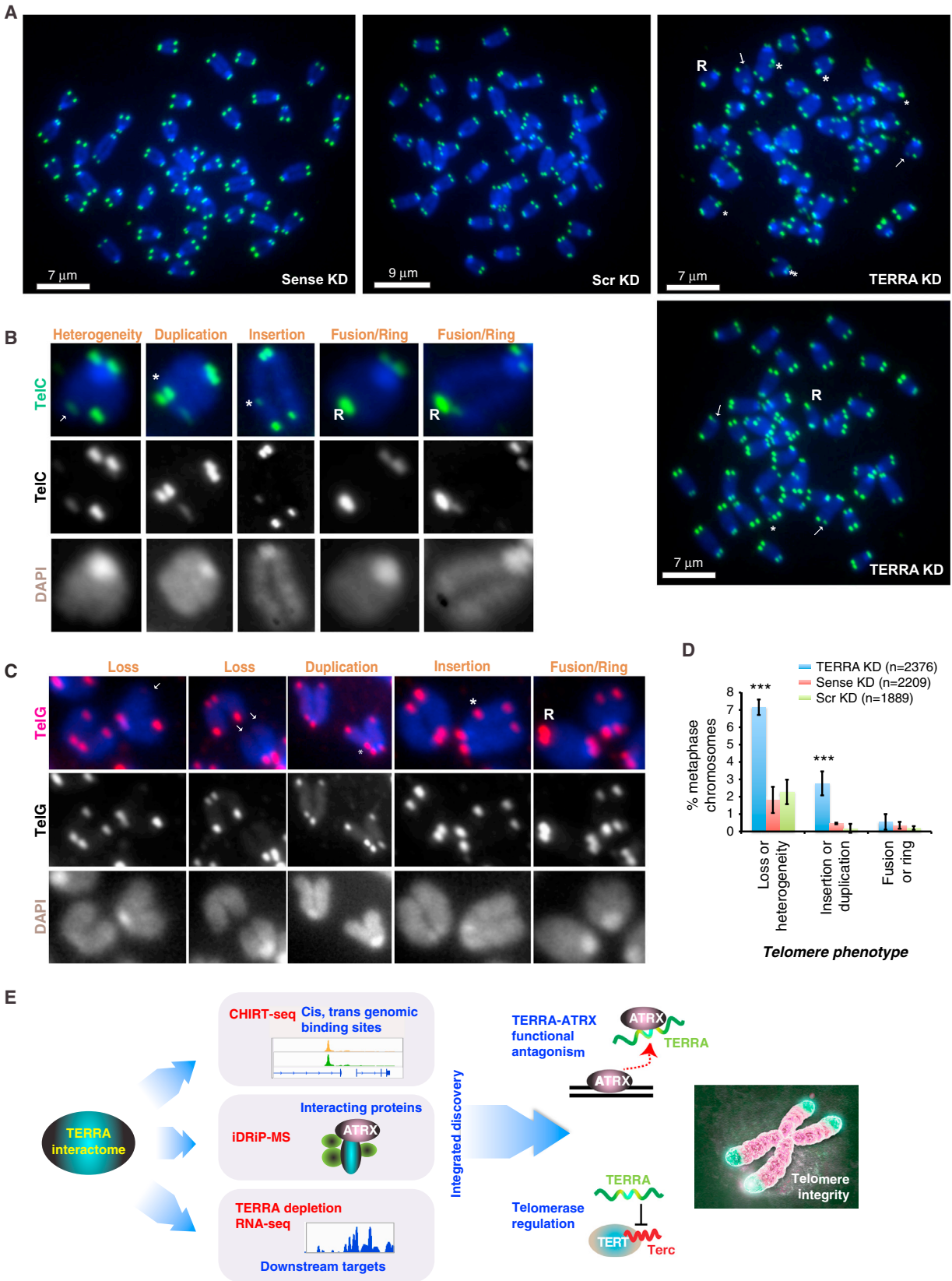
and composition, we efficiently depleted TERRA RNA and reported effects both in *cis* at telomeres (where it is produced) and in *trans* at distant genes. Loss of TERRA results in dysregulation of both subtelomeric genes and internal target genes. Subtelomeric genes appeared to be especially susceptible to TERRA depletion and become downregulated when TERRA is depleted. We have also discovered a large network of TERRA-associated proteins, including epigenetic complexes, telomeric factors, DNA replication proteins, and cell cycle regulators. Among them, ATRX stood out as a major interacting protein partner.

Using orthogonal approaches, we learned that TERRA and ATRX are functionally antagonistic, both at telomeric (*cis*) and non-telomeric (*trans*) sites. Non-telomeric targets comprise a major subclass of TERRA binding sites. When ATRX shares such target genes, ATRX and TERRA are colocalized therein, but exert opposite effects on gene expression: whereas TERRA promotes gene expression, ATRX suppresses it (Figure 4). When TERRA and ATRX do not occur together, TERRA and ATRX could each be either activating or repressive in a manner that likely depends on context-specific interacting partners.

An antagonistic relationship was also apparent at telomeres. TERRA directly binds ATRX and displaces ATRX from telomeric DNA, as evidenced by biochemical analysis using purified factors (Figures 5A–5C). In vivo, TERRA also regulates ATRX association with telomeric chromatin, as a deficiency of TERRA causes increased ATRX localization to telomeres (Figures 5D–5F). We also found that TERRA regulates telomerase activity (Figures 6E–G). TERRA and Terc RNAs associated with each other in vivo and could be pulled down together from UV-cross-linked cell lysates (Figure 6C). This interaction could occur via direct complementarity between TERRA's repeats [5'-(UUAGGG) $_n$ -3'] and the Terc RNA sequence (3'-CAAUCC CAAUC-5'), as suggested previously (Redon et al., 2010); alternatively, TERRA and Terc may simply coexist within a larger complex. Cytological evidence indicated that they do colocalize in vivo (Figure 6D). We also observed that, although the *Terc* locus is not a direct TERRA target, *Terc* RNA levels increase 2-fold in TERRA-depleted cells (Figures 6A and 6B), indicating that telomerase activity is indeed inhibited by TERRA in vivo. This is consistent with prior observations made biochemically in vitro (Schoeftner and Blasco, 2008; Redon et al., 2010; Moravec

### Figure 6. TERRA Associates with Terc and Inhibits Telomerase Activity in ESCs

- (A) RNA-seq of two biological replicates shows that *Terc* is upregulated after TERRA knockdown for 12 hr in ESCs.
- (B) RT-qPCR assay confirms that telomerase RNA is upregulated after TERRA knockdown for 12 hr in ESCs. Error bars, SD.
- (C) TERRA is associated with *Terc* in vivo. RT-qPCR for *Terc* after TERRA capture from UV-cross-linked cell extracts. Control probes for RNA capture: sense, luciferase and U1. Error bars, SD.
- (D) RNA immunoFISH shows that 57% of *Terc* RNA localized with TERRA RNA ( $n = 116$ ). *Terc* also partially colocalized with TRF2 protein, which identifies all telomeric ends.
- (E) Representative TRAP assay validating the increase in telomerase activity upon TERRA knockdown. Three dilutions of the cellular extract are shown. Relative telomerase activity was calculated from the three dilutions. NC, negative control lacking cell extract. An equivalent amount of total cellular protein was used for each sample.
- (F) Linear regression of Ct values and cell extract concentration is shown. Each value represents the average from two biological replicates.
- (G) Relative telomerase activity upon TERRA knockdown (8 hr) determined by RQ-TRAP in ESCs. Values were calculated from two independent biological replicates and three dilutions of each extract shown in (E). SE is indicated ( $n = 6$ ). Values are normalized to total cellular protein.
- (H) Immuno-DNA FISH performed with anti- $\gamma$ H2AX antibodies (red) and telomeric DNA probes (green) shows increased TIF formation in ESCs after TERRA depletion. Arrowheads, TIFs.
- (I) Bar graph showing the number of TIFs with indicated pattern in ESCs following Scr, Sense or TERRA LNA KD. p values (\*\*\*)  $< 0.001$  determined by Fisher Exact test comparing the numbers of nuclei with  $\geq 3$ ,  $\geq 5$ , and  $\geq 8$  TIFs between Scr KD and TERRA KD. n, sample size.



(legend on next page)

et al., 2016). ESCs naturally express high levels of TERRA, consistent with their long telomeres and a need to regulate telomere length. TERRA is known to be regulated in a cell-cycle-dependent manner (Porro et al., 2010), with low levels in late S phase when telomere replication and telomerase recruitment occur (Wellinger et al., 1993; Schmidt et al., 2016). On the other hand, evidence has also shown that TERRA is involved in telomerase recruitment to telomeres and promotes telomere lengthening in yeast (Moravec et al., 2016). Though seemingly contradictory, TERRA-mediated telomerase inhibition and recruitment are not mutually exclusive. TERRA is bound by additional proteins in vivo, and its activity could depend on the exact composition of interactors. A fine balance between Terc and TERRA RNA levels could be vital to telomerase regulation, with an imbalance resulting in telomere instability.

Indeed, TERRA appears to be essential for telomere end protection. Increased telomere dysfunction was observed by TIF assays in ESCs depleted of TERRA (Figures 6H and 6I) (Deng et al., 2009; López de Silanes et al., 2014). Furthermore, various telomeric pathologies were also manifested on metaphase chromosomes after TERRA depletion, including loss of (TTAGGG)<sub>n</sub> sequences from chromosomal ends, insertions and duplications of (TTAGGG)<sub>n</sub> within internal chromosomal regions, and telomeric fusions that form ring-like chromosomal structures (Figure 7). A caveat of note is that telomeres typically have an ~200-base 3' single-strand overhang, on the same G-rich strand as TERRA. Our gapmer ASO could therefore target either TERRA or the DNA overhang and exert the observed effects via either or both, in principle. It is currently not possible to distinguish between these possibilities. However, our sense ASO (LNA) control targeted the C-rich strand of telomeric DNA, not TERRA RNA. The C-rich strand may partially exist in single-stranded form due to engagement in a D-loop and T-loop with the G-rich strand. Given that the sense LNA did not cause increased TIF formation (Figures 6H and 6I) or metaphase chromosome pathology (Figure 7), we favor the idea that the observed effects are at least partially due to depleting TERRA RNA.

In support of TERRA's end-protection function is the proposed antagonistic relationship between TERRA and ATRX (Figures 3–5). ATRX has been known to play a key role in telomere biology (Lovejoy et al., 2012; Doksani and de Lange, 2014). We now know that TERRA and ATRX directly interact (Figure 5). In the context of telomere protection, the antagonistic ATRX-TERRA relationship is especially notable. ATRX suppresses the ALT

pathway that is activated in many cancers to promote telomere lengthening in the absence of telomerase (Lovejoy et al., 2012; Doksani and de Lange, 2014). In tumors lacking telomerase and ATRX function, elongated telomeres are associated with increased TERRA expression (Barthel et al., 2017). We propose that TERRA may be repressing both telomerase expression and ATRX function in these contexts. Thus, apart from protecting chromosomal ends in normal cells, TERRA expression may promote ALT in cancer cells by specifically suppressing ATRX and telomerase. Consistent with this idea, our proteomic analysis identified many other proteins in the ALT pathway, including PML, BLOOM, and SMC5 and SMC6. In the future, the data-rich resources provided by CHIRT and iDRiP can be used to extend analysis of TERRA function in the context of its chromatin and protein interaction networks.

## STAR★METHODS

Detailed methods are provided in the online version of this paper and include the following:

- KEY RESOURCES TABLE
- CONTACT FOR REAGENT AND RESOURCE SHARING
- EXPERIMENTAL MODEL AND SUBJECT DETAILS
- METHOD DETAILS
  - FISH
  - CHIRT-seq
  - TERRA CHIRT-seq analysis
  - ChIP-seq analysis
  - TERRA knockdown
  - RNA-seq analysis
  - Northern blotting analysis
  - Quantitative RT-PCR
  - iDRiP
  - Detection of TERC-TERRA interaction from UV-cross-linked cells
  - Quantitative proteomics
  - Proteomics network and GO analysis
  - Immuno-FISH
  - Electrophoretic mobility shift assay (EMSA)
  - RQ-TRAP and TRAP assays
  - Knockdown ATRX by siRNA
  - Metaphase analysis of telomeric integrity
- QUANTIFICATION AND STATISTICAL ANALYSIS
- DATA AND SOFTWARE AVAILABILITY

### Figure 7. TERRA Maintains Telomere Integrity in ESCs

(A) DNA FISH analysis using telomeric repeat probes of ESC metaphase spreads. Telomeric DNA, green. Metaphase chromosomes, blue. A single cell is shown in each panel. ESCs were harvested after 24 hr knockdown with TERRA LNA versus control (Scr and sense) LNAs. Arrows, loss of telomeric cap on one (heterogeneous) or both sister chromatids. Asterisks, insertion or duplication. R, ring or fused telomeres.

(B) Magnified examples of each aberrant telomere phenotype. DNA FISH performed using C-rich telomeric PNA probes (TelC). Black and white images shown for the TelC and DAPI signals are merged in the color image.

(C) Magnified examples of each aberrant telomere phenotype. DNA FISH performed using G-rich telomeric PNA probes (TelG). Black and white images shown for the TelG and DAPI signals are merged in the color image.

(D) Quantitation of each telomeric pathology. Two biological replicates of each knockdown were averaged. Error bars are SD. \*\*\*p < 0.001, compared to Scr KD. p values determined by two-tailed Chi-square analysis. Number of counted chromosomes is indicated.

(E) Summary: the TERRA interactome revealed by combining CHIRT, iDRiP, and LNA-mediated knockdown enabled determination of TERRA function. TERRA plays a critical role in telomere function by antagonizing ATRX, controlling telomerase activity, and maintaining telomeric integrity. Chromosome image adapted from <http://med.stanford.edu/content/dam/sm-news/images/2015/01/telomeres.jpg>.

## SUPPLEMENTAL INFORMATION

Supplemental Information includes three tables and can be found with this article online at <http://dx.doi.org/10.1016/j.cell.2017.06.017>.

## AUTHOR CONTRIBUTIONS

H-P.C. and J.T.L. conceived of and designed the study. H-P.C. conducted CHIRT, iDRiP, RNA-seq, and immune-FISH analyses. C.C.R. performed EMSA. B.K. and H-P.C. analyzed NGS datasets. H.L. analyzed ATRX ChIP-seq data. E.A. conducted TRAP experiments. H-P.C. and H.J.O. developed CHIRT. C.W. assisted with RNA-seq library preparation, and M.B. and W.H. carried out quantitative proteomic experiments. H-P.C. and J.T.L. wrote the manuscript.

## ACKNOWLEDGMENTS

We thank all members of the lab for valuable discussions and feedback. We also thank C.-S. Wu for advising on IPA software and T. de Lange for discussion. This work is supported by grants from the NIH to J.T.L. (R01-GM58839), and to C.C.R. (K99-GM115868). J.T.L. is an Investigator of the Howard Hughes Medical Institute.

Received: November 30, 2016

Revised: May 26, 2017

Accepted: June 9, 2017

Published: June 29, 2017

## REFERENCES

- Anders, S., Pyl, P.T., and Huber, W. (2015). HTSeq—a Python framework to work with high-throughput sequencing data. *Bioinformatics* *31*, 166–169.
- Azzalin, C.M., and Lingner, J. (2008). Telomeres: the silence is broken. *Cell Cycle* *7*, 1161–1165.
- Azzalin, C.M., and Lingner, J. (2015). Telomere functions grounding on TERRA firma. *Trends Cell Biol.* *25*, 29–36.
- Azzalin, C.M., Reichenbach, P., Khoraiuli, L., Giulotto, E., and Lingner, J. (2007). Telomeric repeat containing RNA and RNA surveillance factors at mammalian chromosome ends. *Science* *318*, 798–801.
- Balk, B., Maicher, A., Dees, M., Klermund, J., Luke-Glaser, S., Bender, K., and Luke, B. (2013). Telomeric RNA-DNA hybrids affect telomere-length dynamics and senescence. *Nat. Struct. Mol. Biol.* *20*, 1199–1205.
- Barthel, F.P., Wei, W., Tang, M., Martinez-Ledesma, E., Hu, X., Amin, S.B., Akdemir, K.C., Seth, S., Song, X., Wang, Q., et al. (2017). Systematic analysis of telomere length and somatic alterations in 31 cancer types. *Nat. Genet.* *49*, 349–357.
- Bernardes de Jesus, B., and Blasco, M.A. (2013). Telomerase at the intersection of cancer and aging. *Trends Genet.* *29*, 513–520.
- Birney, E., Stamatoyannopoulos, J.A., Dutta, A., Guigó, R., Gingeras, T.R., Margulies, E.H., Weng, Z., Snyder, M., Dermitzakis, E.T., Thurman, R.E., et al.; ENCODE Project Consortium; NISC Comparative Sequencing Program; Baylor College of Medicine Human Genome Sequencing Center; Washington University Genome Sequencing Center; Broad Institute; Children's Hospital Oakland Research Institute (2007). Identification and analysis of functional elements in 1% of the human genome by the ENCODE pilot project. *Nature* *447*, 799–816.
- Blackburn, E.H., Greider, C.W., and Szostak, J.W. (2006). Telomeres and telomerase: the path from maize, Tetrahymena and yeast to human cancer and aging. *Nat. Med.* *12*, 1133–1138.
- Chen, L.Y., Majerská, J., and Lingner, J. (2013). Molecular basis of telomere syndrome caused by CTC1 mutations. *Genes Dev.* *27*, 2099–2108.
- Chu, C., Qu, K., Zhong, F.L., Artandi, S.E., and Chang, H.Y. (2011). Genomic maps of long noncoding RNA occupancy reveal principles of RNA-chromatin interactions. *Mol. Cell* *44*, 667–678.
- Cifuentes-Rojas, C., Hernandez, A.J., Sarma, K., and Lee, J.T. (2014). Regulatory interactions between RNA and polycomb repressive complex 2. *Mol. Cell* *55*, 171–185.
- Clynes, D., Jelinska, C., Xella, B., Ayyub, H., Scott, C., Mitson, M., Taylor, S., Higgs, D.R., and Gibbons, R.J. (2015). Suppression of the alternative lengthening of telomere pathway by the chromatin remodelling factor ATRX. *Nat. Commun.* *6*, 7538.
- Cristofari, G., and Lingner, J. (2006). Telomere length homeostasis requires that telomerase levels are limiting. *EMBO J.* *25*, 565–574.
- de Lange, T. (2009). How telomeres solve the end-protection problem. *Science* *326*, 948–952.
- Déjardin, J., and Kingston, R.E. (2009). Purification of proteins associated with specific genomic loci. *Cell* *136*, 175–186.
- Deng, Z., Norseen, J., Wiedmer, A., Riethman, H., and Lieberman, P.M. (2009). TERRA RNA binding to TRF2 facilitates heterochromatin formation and ORC recruitment at telomeres. *Mol. Cell* *35*, 403–413.
- Deng, Z., Wang, Z., Stong, N., Plasschaert, R., Moczan, A., Chen, H.-S., Hu, S., Wikramasinghe, P., Davuluri, R.V., Bartolomei, M.S., et al. (2012). A role for CTCF and cohesin in subtelomere chromatin organization, TERRA transcription, and telomere end protection. *EMBO J.* *31*, 4165–4178.
- Doksani, Y., and de Lange, T. (2014). The role of double-strand break repair pathways at functional and dysfunctional telomeres. *Cold Spring Harb. Perspect. Biol.* *6*, a016576.
- Edwards, A., and Haas, W. (2016). Multiplexed Quantitative Proteomics for High-Throughput Comprehensive Proteome Comparisons of Human Cell Lines. *Methods Mol. Biol.* *1394*, 1–13.
- Elias, J.E., and Gygi, S.P. (2007). Target-decoy search strategy for increased confidence in large-scale protein identifications by mass spectrometry. *Nat. Methods* *4*, 207–214.
- Eng, J.K., McCormack, A.L., and Yates, J.R. (1994). An approach to correlate tandem mass spectral data of peptides with amino acid sequences in a protein database. *J. Am. Soc. Mass Spectrom.* *5*, 976–989.
- Fei, Q., Yang, X., Jiang, H., Wang, Q., Yu, Y., Yu, Y., Yi, W., Zhou, S., Chen, T., Lu, C., et al. (2015). SETDB1 modulates PRC2 activity at developmental genes independently of H3K9 trimethylation in mouse ES cells. *Genome Res.* *25*, 1325–1335.
- Grolimund, L., Aeby, E., Hamelin, R., Armand, F., Chiappe, D., Moniatte, M., and Lingner, J. (2013). A quantitative telomeric chromatin isolation protocol identifies different telomeric states. *Nat. Commun.* *4*, 2848.
- Huang, D.W., Sherman, B.T., and Lempicki, R.A. (2009a). Bioinformatics enrichment tools: paths toward the comprehensive functional analysis of large gene lists. *Nucleic Acids Res.* *37*, 1–13.
- Huang, D.W., Sherman, B.T., and Lempicki, R.A. (2009b). Systematic and integrative analysis of large gene lists using DAVID bioinformatics resources. *Nat. Protoc.* *4*, 44–57.
- Huttlin, E.L., Jedrychowski, M.P., Elias, J.E., Goswami, T., Rad, R., Beausoleil, S.A., Villén, J., Haas, W., Sowa, M.E., and Gygi, S.P. (2010). A tissue-specific atlas of mouse protein phosphorylation and expression. *Cell* *143*, 1174–1189.
- Ishikawa, F., Matunis, M.J., Dreyfuss, G., and Cech, T.R. (1993). Nuclear proteins that bind the pre-mRNA 3' splice site sequence r(UUAG/G) and the human telomeric DNA sequence d(TTAGGG)<sub>n</sub>. *Mol. Cell Biol.* *13*, 4301–4310.
- Kagey, M.H., Newman, J.J., Bilodeau, S., Zhan, Y., Orlando, D.A., van Berkum, N.L., Ebmeier, C.C., Goossens, J., Rahl, P.B., Levine, S.S., et al. (2010). Mediator and cohesin connect gene expression and chromatin architecture. *Nature* *467*, 430–435.
- Kharchenko, P.V., Tolstouk, M.Y., and Park, P.J. (2008). Design and analysis of ChIP-seq experiments for DNA-binding proteins. *Nat. Biotechnol.* *26*, 1351–1359.
- Kim, D., Pertea, G., Trapnell, C., Pimentel, H., Kelley, R., and Salzberg, S.L. (2013). TopHat2: accurate alignment of transcriptomes in the presence of insertions, deletions and gene fusions. *Genome Biol.* *14*, R36.

- Kung, J.T., Colognori, D., and Lee, J.T. (2013). Long noncoding RNAs: past, present, and future. *Genetics* *193*, 651–669.
- Kung, J.T., Kesner, B., An, J.Y., Ahn, J.Y., Cifuentes-Rojas, C., Colognori, D., Jeon, Y., Szanto, A., del Rosario, B.C., Pinter, S.F., et al. (2015). Locus-specific targeting to the X chromosome revealed by the RNA interactome of CTCF. *Mol. Cell* *57*, 361–375.
- Langmead, B., and Salzberg, S.L. (2012). Fast gapped-read alignment with Bowtie 2. *Nat. Methods* *9*, 357–359.
- Law, M.J., Lower, K.M., Voon, H.P., Hughes, J.R., Garrick, D., Viprasakiti, V., Mitson, M., De Gobbi, M., Marra, M., Morris, A., et al. (2010). ATR-X syndrome protein targets tandem repeats and influences allele-specific expression in a size-dependent manner. *Cell* *143*, 367–378.
- Le, P.N., Maranon, D.G., Altina, N.H., Battaglia, C.L., and Bailey, S.M. (2013). TERRA, hnRNP A1, and DNA-PKcs Interactions at Human Telomeres. *Front. Oncol.* *3*, 91.
- Lee, J.T., Davidow, L.S., and Warshawsky, D. (1999). Tsix, a gene antisense to Xist at the X-inactivation centre. *Nat. Genet.* *21*, 400–404.
- López de Silanes, I., Stagno d'Alcontres, M., and Blasco, M.A. (2010). TERRA transcripts are bound by a complex array of RNA-binding proteins. *Nat. Commun.* *1*.
- López de Silanes, I., Graña, O., De Bonis, M.L., Dominguez, O., Pisano, D.G., and Blasco, M.A. (2014). Identification of TERRA locus unveils a telomere protection role through association to nearly all chromosomes. *Nat. Commun.* *5*, 4723.
- Love, M.I., Huber, W., and Anders, S. (2014). Moderated estimation of fold change and dispersion for RNA-seq data with DESeq2. *Genome Biol.* *15*, 550.
- Lovejoy, C.A., Li, W., Reisenweber, S., Thongthip, S., Bruno, J., de Lange, T., De, S., Petrini, J.H., Sung, P.A., Jasin, M., et al.; ALT Starr Cancer Consortium (2012). Loss of ATRX, genome instability, and an altered DNA damage response are hallmarks of the alternative lengthening of telomeres pathway. *PLoS Genet.* *8*, e1002772.
- Maicher, A., Kastner, L., Dees, M., and Luke, B. (2012). Deregulated telomere transcription causes replication-dependent telomere shortening and promotes cellular senescence. *Nucleic Acids Res.* *40*, 6649–6659.
- McAlister, G.C., Huttlin, E.L., Haas, W., Ting, L., Jedrychowski, M.P., Rogers, J.C., Kuhn, K., Pike, I., Grothe, R.A., Blethrow, J.D., and Gygi, S.P. (2012). Increasing the multiplexing capacity of TMTs using reporter ion isotopologues with isobaric masses. *Anal. Chem.* *84*, 7469–7478.
- McAlister, G.C., Nusinow, D.P., Jedrychowski, M.P., Wühr, M., Huttlin, E.L., Erickson, B.K., Rad, R., Haas, W., and Gygi, S.P. (2014). MultiNotch MS3 enables accurate, sensitive, and multiplexed detection of differential expression across cancer cell line proteomes. *Anal. Chem.* *86*, 7150–7158.
- Minajigi, A., Froberg, J.E., Wei, C., Sunwoo, H., Kesner, B., Colognori, D., Lessing, D., Payer, B., Boukhali, M., Haas, W., and Lee, J.T. (2015). Chromosomes. A comprehensive Xist interactome reveals cohesin repulsion and an RNA-directed chromosome conformation. *Science* *349*.
- Moravec, M., Wischniewski, H., Bah, A., Hu, Y., Liu, N., Lafranchi, L., King, M.C., and Azzalin, C.M. (2016). TERRA promotes telomerase-mediated telomere elongation in *Schizosaccharomyces pombe*. *EMBO Rep.* *17*, 999–1012.
- Pfeiffer, V., and Lingner, J. (2012). TERRA promotes telomere shortening through exonuclease 1-mediated resection of chromosome ends. *PLoS Genet.* *8*, e1002747.
- Pinter, S.F., Sadreyev, R.I., Yildirim, E., Jeon, Y., Ohsumi, T.K., Borowsky, M., and Lee, J.T. (2012). Spreading of X chromosome inactivation via a hierarchy of defined Polycomb stations. *Genome Res.* *22*, 1864–1876.
- Porro, A., Feuerhahn, S., Reichenbach, P., and Lingner, J. (2010). Molecular dissection of telomeric repeat-containing RNA biogenesis unveils the presence of distinct and multiple regulatory pathways. *Mol. Cell. Biol.* *30*, 4808–4817.
- Quinlan, A.R., and Hall, I.M. (2010). BEDTools: a flexible suite of utilities for comparing genomic features. *Bioinformatics* *26*, 841–842.
- Redon, S., Reichenbach, P., and Lingner, J. (2010). The non-coding RNA TERRA is a natural ligand and direct inhibitor of human telomerase. *Nucleic Acids Res.* *38*, 5797–5806.
- Rippe, K., and Luke, B. (2015). TERRA and the state of the telomere. *Nat. Struct. Mol. Biol.* *22*, 853–858.
- Sandell, L.L., Gottschling, D.E., and Zakian, V.A. (1994). Transcription of a yeast telomere alleviates telomere position effect without affecting chromosome stability. *Proc. Natl. Acad. Sci. USA* *91*, 12061–12065.
- Sarma, K., Cifuentes-Rojas, C., Ergun, A., Del Rosario, A., Jeon, Y., White, F., Sadreyev, R., and Lee, J.T. (2014). ATRX directs binding of PRC2 to Xist RNA and Polycomb targets. *Cell* *159*, 869–883.
- Scheibe, M., Arnoult, N., Kappei, D., Buchholz, F., Decottignies, A., Butter, F., and Mann, M. (2013). Quantitative interaction screen of telomeric repeat-containing RNA reveals novel TERRA regulators. *Genome Res.* *23*, 2149–2157.
- Schmidt, J.C., Zaugg, A.J., and Cech, T.R. (2016). Live Cell Imaging Reveals the Dynamics of Telomerase Recruitment to Telomeres. *Cell* *166*, 1188–1197.e9.
- Schoeftner, S., and Blasco, M.A. (2008). Developmentally regulated transcription of mammalian telomeres by DNA-dependent RNA polymerase II. *Nat. Cell Biol.* *10*, 228–236.
- Shin, H., Liu, T., Manrai, A.K., and Liu, X.S. (2009). CEAS: cis-regulatory element annotation system. *Bioinformatics* *25*, 2605–2606.
- Simon, M.D., Wang, C.I., Kharchenko, P.V., West, J.A., Chapman, B.A., Alekseyenko, A.A., Borowsky, M.L., Kuroda, M.I., and Kingston, R.E. (2011). The genomic binding sites of a noncoding RNA. *Proc. Natl. Acad. Sci. USA* *108*, 20497–20502.
- Ting, L., Rad, R., Gygi, S.P., and Haas, W. (2011). MS3 eliminates ratio distortion in isobaric multiplexed quantitative proteomics. *Nat. Methods* *8*, 937–940.
- Trapnell, C., Hendrickson, D.G., Sauvageau, M., Goff, L., Rinn, J.L., and Pachter, L. (2013). Differential analysis of gene regulation at transcript resolution with RNA-seq. *Nat. Biotechnol.* *31*, 46–53.
- Webb, C.J., and Zakian, V.A. (2016). Telomerase RNA is more than a DNA template. *RNA Biol.* *13*, 683–689.
- Wellinger, R.J., Wolf, A.J., and Zakian, V.A. (1993). Origin activation and formation of single-strand TG1-3 tails occur sequentially in late S phase on a yeast linear plasmid. *Mol. Cell. Biol.* *13*, 4057–4065.
- Yu, T.Y., Kao, Y.W., and Lin, J.J. (2014). Telomeric transcripts stimulate telomere recombination to suppress senescence in cells lacking telomerase. *Proc. Natl. Acad. Sci. USA* *111*, 3377–3382.
- Zhang, Y., Liu, T., Meyer, C.A., Eeckhoutte, J., Johnson, D.S., Bernstein, B.E., Nussbaum, C., Myers, R.M., Brown, M., Li, W., and Liu, X.S. (2008). Model-based analysis of ChIP-Seq (MACS). *Genome Biol.* *9*, R137.
- Zhang, L.-F., Ogawa, Y., Ahn, J.Y., Namekawa, S.H., Silva, S.S., and Lee, J.T. (2009). Telomeric RNAs mark sex chromosomes in stem cells. *Genetics* *182*, 685–698.

## STAR★METHODS

## KEY RESOURCES TABLE

REAGENT or RESOURCE	SOURCE	IDENTIFIER
<b>Antibodies</b>		
Rabbit polyclonal anti-ATRX	Santa Cruz	Cat#sc-15408; RRID: AB_2061023
Rabbit polyclonal anti-TRF2	Santa Cruz	Cat#sc-9143; RRID: AB_220133
Rabbit polyclonal anti-RAP1	Santa Cruz	Cat#sc-28197; RRID: AB_2269341
Mouse monoclonal anti-phospho-Histone H2A.X (Ser139)	EMD Millipore	Cat#05-636
Rabbit monoclonal anti-GAPDH (14C10)	Cell Signaling	Cat#2118; RRID: AB_561053
<b>Chemicals, Peptides, and Recombinant Proteins</b>		
ULTRAhyb-Oligo hybridization buffer	Thermo Fisher Scientific	Cat#AM8663
TURBO DNase	Thermo Fisher Scientific	Cat#AM2239
MyOne streptavidin C1 beads	Thermo Fisher Scientific	Cat#65001
TMT-10plex reagents	Thermo Fisher Scientific	Cat#90110
iTaq Universal SYBR Green Supermix	Bio-Rad	Cat#4472908
Agencourt AMPure XP	Beckman Coulter	Cat#A63881
Superscript III Reverse Transcriptase	Thermo Fisher Scientific	Cat#8080044
RNase H	New England Biolabs	Cat#M0297L
RNaseA	Thermo Fisher Scientific	Cat#12091021
Proteinase K	Sigma-Aldrich	Cat#03115844001
TRIzol	Thermo Fisher Scientific	Cat#15596018
Yeast RNA	Thermo Fisher Scientific	Cat#AM7118
SUPERase• In RNase Inhibitor	Thermo Fisher Scientific	Cat#AM2694
T4 polynucleotide kinase	New England Biolabs	Cat#M0201S
T4 DNA polymerase	New England Biolabs	Cat#M0203S
ATRX protein	(Sarma et al., 2014)	N/A
Glutaraldehyde solution	Sigma-Aldrich	Cat#G5882-10X10ML
Protector RNase Inhibitor	Roche	Cat#03335399001
Paraformaldehyde solution	Thermo Fisher Scientific	Cat#50980492
lipofectamine RNAiMAX	Thermo Fisher Scientific	Cat#13778030
Dextran Sulfate	EMD Millipore	Cat#S4030
Formamide	American Bioanalytical	Cat#AB00600-00500
LIF	EMD Millipore	Cat#ESG1106
2-Mercaptoethanol	Thermo Fisher Scientific	Cat#21985023
MEM NEAA	Thermo Fisher Scientific	Cat#11140076
HEPES	Thermo Fisher Scientific	Cat#15630130
GlutaMAX-1	Thermo Fisher Scientific	Cat#35050079
<b>Critical Commercial Assays</b>		
NEBNext Multiplex Oligos for Illumina	New England Biolabs	Cat#E7335S
NEBNext ChIP-Seq Library Prep Master Mix Set for Illumina	New England Biolabs	Cat#E6240S
NEBNext mRNA Second Strand Synthesis Module	New England Biolabs	Cat#E6111S
mirVana miRNA Isolation Kit	Thermo Fisher Scientific	Cat#AM1561
Ribominus Eukaryote Kit v2	Thermo Fisher Scientific	Cat#A15020
Quant-iT PicoGreen dsDNA Reagent	Thermo Fisher Scientific	Cat#P7581

(Continued on next page)

**Continued**

REAGENT or RESOURCE	SOURCE	IDENTIFIER
Mouse ES Cell Nucleofector Kit	Lonza-Walkersville	Cat#VVPH-1001
RNeasy MinElute Cleanup kit	QIAGEN	Cat#74204
Deposited Data		
TERRA CHIRT-seq and RNA-seq	This paper	GEO: GSE79180
Mouse reference genome GRCm38/mm10	Genome Reference Consortium	<a href="https://www.ncbi.nlm.nih.gov/grc/mouse">https://www.ncbi.nlm.nih.gov/grc/mouse</a>
ATRX ChIP-seq	(Law et al., 2010)	GEO: GSM551138
CTCF ChIP-seq	(Kung et al., 2015)	GEO: GSM1540992
Ezh2 ChIP-seq	(Pinter et al., 2012)	GEO: GSM905437
PollIS5 ChIP-seq	(Pinter et al., 2012)	GEO: GSM905442
H3K4me3 ChIP-seq	(Pinter et al., 2012)	GEO: GSM905439
H3K9me3 ChIP-seq	(Fei et al., 2015)	GEO: GSM1531184
H3K27me3 ChIP-seq	(Pinter et al., 2012)	GEO: GSM905438
SMC1 ChIP-seq	(Kagey et al., 2010)	GEO: GSM560341
H3K36me3 ChIP-seq	(Pinter et al., 2012)	GEO: GSM905441
Experimental Models: Cell Lines		
Mouse embryonic stem cells (female,16.7) Strain: <i>M. castaneus</i> x <i>M. musculus</i>	(Lee et al., 1999)	N/A
Sequence-Based Reagents		
TERRA FISH probe: (TAACCC) <sub>7</sub> -Alexa488-3'	Integrated DNA Technologies	N/A
TelC-Alexa488 PNA probe: CCCTAACCCCTAACCCCTAA	PNA Bio Inc	Cat#1004
TelG-Cy3 PNA probe: TTAGGGTTAGGGTTAGGG	PNA Bio Inc	Cat#1006
Northern probe TERRA: 5'-(TAACCC) <sub>5</sub> -3'	Integrated DNA Technologies	N/A
Northern probe GAPDH: 5'-GTAGACCCACGACATA CTCAGCACCGGCTCACCCATT-3'	Integrated DNA Technologies	N/A
ATRX siRNA-1, Sense 5'-GGACUUCAUGGGAUC GUGAtt-3'; Antisense 5'-UCACGAUCCCAUGAA GUCCat-3'	Thermo Fisher Scientific	Cat#4390771; siRNA ID#s76136
ATRX siRNA-2, Sense 5'-GGCGCAUUAAGGUUCAA GAtt-3'; Antisense 5'-UCUUGAACCUUAAUGCGCCgt-3'	Thermo Fisher Scientific	Cat#4390771; siRNA ID#s76137
Control siRNA, Silencer Select Negative Control No. 1	Thermo Fisher Scientific	Cat#4390843
PCR primers for spike-in control Lambda DNA, F: 5'-GCATATGTTGTGTTTACAG-3'; R: 5'-GCAAC AAATTGATAAGCA-3'	Thermo Fisher Scientific	N/A
LNA gapmer Scr: 5'-CACGTCTATACACCAC-3'	Exiqon	N/A
LNA gapmer TERRA: 5'-TAACCCTAACCCCTAAC-3'	Exiqon	N/A
LNA gapmer Sense: 5'-TTA GGG TTA GGG TTA G-3'	Exiqon	N/A
3' biotin-TEG Luciferase probe sequence: 5'-GTAT CCCTGGAAGATGGAAG-3'	Integrated DNA Technologies	N/A
3' biotin-TEG TERRA-AS probe sequence: 5'-TAA CCCTAACCCCTAACCCCTA-3'	Integrated DNA Technologies	N/A
3' biotin-TEG TERRA-sense probe sequence: 5'-TTA GGGTTAGGGTTAGGGTT-3'.	Integrated DNA Technologies	N/A
3' biotin-TEG U1 probe sequence: 5'-CTCCCCTGCC AGGTAAGTAT-3'	Integrated DNA Technologies	N/A
TRAP assay primers, ACX: 5'-GCGCGCTTACCC TTACCCTTACCCTAACCC-3'; TS: 5'-AATCCGTGCA GCAGAGTT-3'	Integrated DNA Technologies	N/A
For EMSA, TERRA RNA (30 nt): 5'-UUAGGGUU AGGGUUAGGGUUAGGGUUAGGG-3'	Integrated DNA Technologies	N/A

(Continued on next page)

**Continued**

REAGENT or RESOURCE	SOURCE	IDENTIFIER
For EMSA, U1 RNA (30nt): 5'-AUACUUACCUAGG CAGGGGAGAUACCAUGAU-3'	Integrated DNA Technologies	N/A
For EMSA, ssDNA telomeric DNA (30 nt): 5'-(GGGTTA) <sub>5</sub> -3'	Integrated DNA Technologies	N/A
For EMSA, ssDNA telomeric DNA (80 nt): 5'-(GGGTTA) <sub>13</sub> GG-3'	Integrated DNA Technologies	N/A
For EMSA, In vitro transcription for TERRA (83 nt): 5'-AACCC(TAACCC) <sub>13</sub> TATAGTGAGTCGTATTA-3'	Integrated DNA Technologies	N/A
For EMSA, In vitro transcription for U1 (83 nt): 5'-CGCAGGGGTGAGCAGCATCCGGAGTGCAATGGA TAA GCCTCGCCCTGGGAAAACACCTTCGTGA TCATGGTATCTCCCCTGCCTATAGTGAGTCGTA TTA-3'	Integrated DNA Technologies	N/A
For EMSA, T7 oligo: 5'-TAATACGACTCACTATA-3'	Integrated DNA Technologies	N/A
For qRT-PCR primers, please see <a href="#">Table S3</a>	Integrated DNA Technologies	N/A

## Software and Algorithms

Bowtie2	(Langmead and Salzberg, 2012)	<a href="http://bowtie-bio.sourceforge.net/bowtie2/index.shtml">http://bowtie-bio.sourceforge.net/bowtie2/index.shtml</a>
TopHat2	(Kim et al., 2013)	<a href="https://ccb.jhu.edu/software/tophat/index.shtml">https://ccb.jhu.edu/software/tophat/index.shtml</a>
Bedtools	(Quinlan and Hall, 2010)	<a href="http://bedtools.readthedocs.io/en/latest/">http://bedtools.readthedocs.io/en/latest/</a>
Trim Galore	Babraham Bioinformatics	<a href="http://www.bioinformatics.babraham.ac.uk/projects/trim_galore/">http://www.bioinformatics.babraham.ac.uk/projects/trim_galore/</a>
NovoAlign (v3.00.02)	Novocraft	<a href="http://www.novocraft.com/products/novoalign/">http://www.novocraft.com/products/novoalign/</a>
SPP	(Kharchenko et al., 2008)	<a href="https://sites.google.com/a/brown.edu/bioinformatics-in-biomed/spp-r-from-chip-seq">https://sites.google.com/a/brown.edu/bioinformatics-in-biomed/spp-r-from-chip-seq</a>
MACS (1.4.2)	(Zhang et al., 2008)	<a href="http://liulab.dfci.harvard.edu/MACS/">http://liulab.dfci.harvard.edu/MACS/</a>
CEAS	(Shin et al., 2009)	<a href="http://liulab.dfci.harvard.edu/CEAS/usermanual.html">http://liulab.dfci.harvard.edu/CEAS/usermanual.html</a>
HTSeq	(Anders et al., 2015)	<a href="http://www-huber.embl.de/users/anders/HTSeq/doc/overview.html">http://www-huber.embl.de/users/anders/HTSeq/doc/overview.html</a>
DESeq2	(Love et al., 2014)	<a href="http://www.bioconductor.org/packages/release/bioc/html/DESeq2.html">http://www.bioconductor.org/packages/release/bioc/html/DESeq2.html</a>
Cuffdiff 2	(Trapnell et al., 2013)	<a href="http://cole-trapnell-lab.github.io/cufflinks/">http://cole-trapnell-lab.github.io/cufflinks/</a>
Ingenuity Pathway Analysis	QIAGEN	<a href="https://www.ingenuity.com/products/ipa">https://www.ingenuity.com/products/ipa</a>
DAVID Bioinformatics Resources 6.7	(Huang et al., 2009b)	<a href="https://david.ncifcrf.gov/">https://david.ncifcrf.gov/</a>

**CONTACT FOR REAGENT AND RESOURCE SHARING**

Further information and requests for reagents should be directed to the Lead Contact, Jeannie T. Lee ([lee@molbio.mgh.harvard.edu](mailto:lee@molbio.mgh.harvard.edu)).

**EXPERIMENTAL MODEL AND SUBJECT DETAILS**

Mouse embryonic stem cells were cultured in regular ES medium (500 mL DMEM with addition of 1 mL of  $\beta$ -mercaptoethanol, 6 mL of MEM NEAA, 25 mL of 7.5% NaHCO<sub>3</sub>, 6 mL of GlutaMAX-1, 15 mL of 1M HEPES, 90 mL of FBS, 300  $\mu$ L of LIF, 6 mL of PEN/STREP) with feeders.

**METHOD DETAILS****FISH**

Cells were cytospun onto glass slides and permeabilized with CSK buffer containing 0.5% Triton X-100, and fixed in 4% paraformaldehyde. DNA oligos probes for RNA FISH were ordered from Integrated DNA Technologies. For TERRA: (TAACCC)<sub>7</sub>-Alexa488-3'.

DNA oligo probes for RNA-FISH were mixed at the final concentration 0.5 pmol/ $\mu$ l in hybridization solution (50% formamide, 2  $\times$  SSC, 2 mg/ml BSA, 10% Dextran Sulfate-500K). Hybridization was carried out at 42°C overnight for RNA FISH. Slides were washed with 2  $\times$  SSC/50% formamide for 5 min three times at 44°C, and then wash with 2  $\times$  SSC for 5 min twice at 44°C.

### CHIRT-seq

Since TERRA transcripts contain repetitive sequences and have different subtelomeric sequences, it is impractical to use tiling probes to capture TERRA RNA. Thus, we developed CHIRT-seq protocol to specifically capture TERRA RNA with one single oligo probe that targets telomeric repeat sequence. This protocol also has an advantage for mapping the binding sites of other repetitive RNAs or short RNAs on the genome.

The TERRA CHIRT protocol includes specific features that differ from the original ChIRP and CHART protocols (Chu et al., 2011; Simon et al., 2011) as following. (i) We used only one probe to capture RNAs and it reduced the chance of off-target effects compared to using multiple probes. (ii) We decreased the shearing intensity to preserve integrity of long noncoding RNAs. (iii) We increased the specificity of RNA-mediated capture by improving the elution steps. Because we observed that RNaseH is not active in SDS buffer, we used NP40 instead of SDS or N-lauroyl sarcosine in the final DNA elution to better preserve RNaseH activity. (iiii) We included the spike-in control DNA before library construction, and it allowed a proper normalization between samples. In this way, we can compare the enrichment on the repetitive sequence regions, or on whole genomic coverage from different cellular conditions.

Specifically, mouse ESCs were grown to 80% confluency and feeder cells were removed. 15 millions of cells were spun down and washed with PBS once. Cells were resuspended in 10 mL of PBS and then another 10 mL of 2% of glutaraldehyde were added to fix cells at room temperature for 10 min. Crosslinking was then quenched with 0.125 M glycine for 5 min. Followed by two washes with cold PBS, cell pellets were immediately frozen in liquid nitrogen and stored at  $-80^{\circ}\text{C}$ . Cells were thawed out on ice, and were resuspended in 1 mL of swelling buffer (0.1 M Tris pH 7.0, 10 mM KOAc, 15 mM MgOAc, 1% NP40, 1mM DTT, 1mM PMSF, 100 U/ml Superase-In[Ambion]) for 10 min on ice. Cells were then dounced and pelleted at 2500 g for 5 min. Nuclei was further lysed in nuclear lysis buffer (50 mM Tris pH7.0, 10 mM EDTA, 1% SDS, 1mM DTT, 1mM PMSF, protease inhibitor, 100 U/ml Superase-In) on ice for 10 min, and sonicated using Bioruptor until DNA size 0.5-3 kb (it usually takes 1.5 hr and depends on the cell numbers). Cell lysates were then spun down at 13,000 rpm for 5 min to remove insoluble debris. Cell lysates were then frozen in liquid nitrogen and stored in  $-80^{\circ}\text{C}$ . Streptavidin- magnetic C1 (Thermo Fisher) beads were blocked with 500 ng/ $\mu$ l yeast total RNA, and 1mg/ml BSA for 1 hr at 37°C, and resuspended in 1X hybridization buffer (1 volume of lysis buffer plus 2 volume of 2X hybridization buffer). Cell lysates were diluted in two times volume of 2X hybridization buffer (750 mM NaCl, 1% SDS, 50 mM Tris pH 7.0, 1 mM EDTA, 15% Formamide, 1 mM DTT, PMSF, protease inhibitor, and 100 U/ml Superase-In), and were precleaned with Streptavidin- magnetic C1 beads at 37°C for 1 hr (100  $\mu$ L of beads for 1 mL lysates). Precleaned lysates were incubated with probes (100 pmol for 3 mL of diluted cell lysates) at 37°C for 3 hr. Three hundred microliters washed/blocked C1 beads were added per 100 pmol of probes, and the whole reaction was mixed for another 1 hr at 37°C. DNA probes for CHIRT were ordered from Integrated DNA Technologies and labeled with 3' biotin-TEG. Beads:biotin-probes:RNA:chromatin adducts were washed five times at 37°C for 5 min with wash buffer (2X SSC, 0.5% SDS, 1 mM DTT, 1 mM PMSF), and then washed twice for 5 min at room temperature with 0.1% NP40 buffer (150 mM NaCl, 50 mM Tris pH8.0, 3 mM MgCl<sub>2</sub>, 10 mM DTT, 0.1% NP40). DNA was then eluted twice for 20 min in 450  $\mu$ L of 0.1% NP40 buffer with 200 U/ml RNaseH (NEB) at room temperature. DNA for no RNaseH controls was eluted in 0.1% NP40 buffer without RNaseH. Eluted DNA was treated with RNaseA (1 mg/ml) at 37°C for 1 hr, and then was treated with proteinase K (1 mg/ml) and supplied addition of SDS to 0.5% at final concentration at 55°C for 16 hr. DNA was extracted with phenol/chloroform using phase lock gel tubes. For pre-RNaseA treatment control, cell lysates were treated with RNaseA at 37°C overnight before hybridization. For RNA elution after hybridization, beads:biotin-probes:RNA:chromatin adducts were washed 5 time in wash buffer, then treated with proteinase K in PK buffer (100 mM NaCl, Tris pH 7.0, 1 mM EDTA, 0.5% SDS) at 55°C for 30 min. Beads-suspension was boiled at 90°C for 5 min, and then RNA was extracted using TRIzol (ThermoFisher).

### TERRA CHIRT-seq analysis

PicoGreen (ThermoFisher) was used to estimate the concentration of eluted DNA. Before library construction, equal amount of lambda DNA (0.015 pg of PCR products,  $\sim$ 250bp) was added as spike-in control into eluted DNA samples. Lambda DNA PCR products were used as spike-in control. Following the removal of adaptor sequences and PCR duplicates, paired-end 50 bp sequencing data was aligned to mouse reference genome (GRCm38/mm10 and NCBI37/mm9) using the software Novoalign (v3.00.02) (<http://www.novocraft.com/products/novoalign/>). The coverage files were generated using R software library SPP software (Kharchenko et al., 2008) with smoothing using 500 bp bins with a 100 bp step size to generate control-subtracted, normalized read densities. Controls include input, sense-CHIRT, and TERRA-CHIRT without RNaseH elution (no RNaseH). These data were visualized using IGV software to display all tracks with a mean windowing function and scales indicated in each figure. Other methods to generate normalized coverage files, including the generation of conservative enrichment and maximum likelihood estimates, resulted in similar distribution patterns. Scatterplots for correlation analysis used input-normalized coverage produced by SPP, windowed by 3 kb bins and filtered out unenriched bins with an averaged density smaller than 4. Peaks were called by MACS (1.4.2) (Zhang et al., 2008) software using normalization to indicated controls (e.g., input, sense, no RNaseH or pre-RNaseA), and filtered by 10-fold enrichment and the length greater than 1kb as shown in Figure 1E. Metagene profiles were produced by software CEAS (0.9.9.7) (Shin et al., 2009) using 2 fold enriched over input wig files and bed files produced by MACS peak calling. For comparison to TERRA KD

RNA-seq data, plus-peaks genes flanking  $\pm$  10kb with TERRA peaks (20-fold enriched from MACS peak calling) were selected, and minus-peaks genes (non-targets) were the rest of genes.

### ChIP-seq analysis

For comparison to other ChIP-seq datasets, we analyzed published datasets: ATRX (GSM551138)([Law et al., 2010](#)), CTCF (GSM1540992)([Kung et al., 2015](#)), Ezh2 (GSM905437)([Pinter et al., 2012](#)), Polr1b (GSM905442) ([Pinter et al., 2012](#)), H3K4me3 (GSM905439) ([Pinter et al., 2012](#)), H3K9me3 (GSM1531184) ([Fei et al., 2015](#)), H3K27me3 (GSM905438) ([Pinter et al., 2012](#)), SMC1 (GSM560341) ([Kagey et al., 2010](#)) and H3K36me3 (GSM905441) ([Pinter et al., 2012](#)). Fastq files were aligned to the mm10 genome using Bowtie2 (-k 1 -very-sensitive -no-disordant) ([Langmead and Salzberg, 2012](#)). Peak calling software Macs2 (version 1.4.2 20120305 or greater, with either -BAMPE or -BAM option) was used to select peaks with  $p = 0.05$  or less. Peaks from the resultant xls files were converted to wiggle format (MARK.WIG) with peak amplitude set to 1 giving each called nucleotide an equal weight. Metagene analysis around TERRA ChIRT peaks was determined using software CEAS (sitepro 0.6.6) (package version 1.0.2) ([Shin et al., 2009](#)) with arguments (-w MARK.WIG -b TER\_PEAKS.bed -span = 3000) for each mark. TER\_PEAKS.bed included macs2 selected TERRA peaks with  $p$  value  $\leq 0.05$  and FDR  $\leq 0.05$  aligned to mm10. Bed region intersect was used to obtain counts for intersecting peaks between TERRA peaks and the above marks, converted from Mac2 XLS format to BED format with PCR dups removed. Intersection is done using bedtools intersect ([Quinlan and Hall, 2010](#)) (version 2.15.0, parameters -wb -f 0.5 -a MARK.bed -b TER\_PEAKS.bed) and intersecting regions dups removed and counted.

### TERRA knockdown

Mouse ESCs (female, 16.7, cas/mus hybrid) were grown to 70% confluency, and then trypsinized, and feeder cells were removed. A total of  $2 \times 10^6$  ESCs were transfected with LNA gapmer oligos at a concentration of 2~8  $\mu$ M in 100  $\mu$ L nucleofector solution using A30 program (nucleofector kits, Lonza). A total of 2 mL of feeders-conditional medium (medium from feeders grown in mES medium for 6-18 hr) was added to the cells, and the cells were plated on gelatinized plates. TERRA and Sense LNA gapmers were designed and synthesized by Exiqon ([www.exiqon.com](http://www.exiqon.com)) with modified LNA bases and phosphothiolated backbone modification.

### RNA-seq analysis

Cells were all tested and confirmed that they were free from mycoplasma contamination. Total RNA was isolated using TRIzol (ThermoFisher), depleted of DNA by DNase treatment (TURBO DNase, Ambion), depleted of ribosomal RNA (Ribominus Eukaryote Kit v2, ThermoFisher), purified greater than 200 nucleotides using mirVana RNA extraction kit (ThermoFisher), and fragmented in first strand synthesis buffer (NEB) containing magnesium at 95°C for 10 min to a median size 150-200 bp. cDNA was reverse transcribed with random primers (with Actinomycin D) using Superscript III (ThermoFisher) at 50°C for 30 min. The following steps such as second strand synthesis, end repair, dA-tailing, adaptor ligation, USER enzyme digestion, double size selection (0.6x-1.2x AMPure XP beads), and library amplification were performed according to NEBUltra Directional RNA library preparation protocol for Illumina (NEB). Sequencing of purified libraries was carried out on an Illumina HiSeq instrument for paired 50 nucleotides reads. After removal of adaptor sequences by Trim Galore, reads were aligned to mouse genomes (GRCm38/mm10 and NCBI37/mm9) using Tophat2 ([Kim et al., 2013](#)). After removal of PCR duplicates, data were analyzed using Cuffdiff 2 ([Trapnell et al., 2013](#)). Differential expression was presented as delta FPKM (fragments per kilobase million of exon per million fragment mapped) values comparing TERRA and Scr LNA knockdown samples using Cuffdiff 2. Two biological replicates were analyzed. Coverage of RNA-seq was normalized by per million mapped reads as FPM value shown in the tracks. For DESeq2 analysis ([Love et al., 2014](#)), raw counts were generated by HTSeq ([Anders et al., 2015](#)), and the significantly differentially expressed genes were identified by P-adj values  $< 0.05$ .

### Northern blotting analysis

All oligo probes were end labeled using T4 polynucleotide kinase. Total RNA was extracted using TRIzol followed by acid phenol extraction. Total RNA (5  $\mu$ g) was loaded in each lane. Hybridization was carried out at 42°C overnight using ULTRAhyb-Oligo hybridization buffer (ThermoFisher).

### Quantitative RT-PCR

Total RNA was isolated using TRIzol (ThermoFisher), treated with TURBO DNase (ThermoFisher), and reverse-transcribed with random primers using Superscript III reverse transcriptase (ThermoFisher). RT-qPCR was performed using iQ SYBR Green Supermix (Bio-Rad). Expression levels were normalized to GAPDH levels.

### iDRiP

The iDRiP technology provides a simple and high specificity way to investigate the direct RNA-protein interaction in vivo, and will be beneficial for the investigation of the RNA-protein interactome for almost any types of RNAs including repetitive RNAs or short RNAs. Compare to other RNA capture proteomic analysis ([Chu et al., 2011](#)), we reduced the background of DNA-mediated protein interaction by applying the additional DNase treatment on the wash steps. We also included more controls such as sense probe, U1 and luciferase for proper normalization of quantitative proteomics. TERRA iDRiP protocol improved the signal-to-noise ratio by optimization of hybridization and washing condition compared to the original iDRiP method ([Minajigi et al., 2015](#)).

After removing feeders, mouse embryonic stem cells ( $15 \times 10^7$  cells) were irradiated with UV light at 400 mJ energy (Stratagene 2400) in cold PBS, cells were treated with CSKT-0.5% (10 mM PIPES, pH 6.8, 100 mM NaCl, 3 mM  $MgCl_2$ , 0.3 M sucrose, 0.5% Triton X-100, 1 mM PMSF) for 10 min at 4°C followed by a spin. Snap freezing cells could be stored at  $-80^\circ C$ . Crosslinked cells were re-suspended in 3 mL of DNase I digestion buffer (50 mM Tris pH 7.5, 0.5% Nonidet-P 40, 0.1% sodium lauroyl sarcosine, 1x protease inhibitors, Superaseln, 600U DNase I, 10 mM vanadyl ribonucleoside complex). The tubes were incubated at 37°C water bath for 15 min with rotations. The nuclear lysates were further supplied to the final concentrations of 1% sodium lauroyl sarcosine, 0.1% sodium deoxycholate, 0.5 M lithium chloride, 25 mM EDTA and 25 mM EGTA and incubated at 37°C for 5 min. The lysates were spun and the supernatants were collected. The pellets were resuspended in 300  $\mu L$  of lysis buffer (50 mM Tris pH 7.5, 0.5M LiCl, 1% Nonidet-P 40, 1% sodium lauroyl sarcosine, 0.1% sodium lauroyl sarcosine, 20 mM EDTA, 20mM EGTA), incubated on ice for 10 min, heated to 65°C for 5 min, immediately spun at room temperature for 1 min, and stored on ice. The supernatants were collected and combined with the previous supernatants. The combined supernatants were pre-cleaned by incubation with MyOne streptavidin C1 beads (ThermoFisher, 50  $\mu L$  beads for 3.5ml of lysate) at room temperature for 20 min, and beads were removed. To conjugate DNA probes to beads, 160  $\mu L$  of beads was incubated with 80 pmole of probes in 2X binding buffer (10 mM Tri-HCl (pH7.5), 1 mM EDTA, 2 M NaCl) at room temperature for 20 min, washed with 1X binding buffer twice, and then resuspended in 160  $\mu L$  of lysis buffer. Pre-cleaned lysate and probes-conjugated beads were pre-heated to 65°C for 5 min, mixed together and incubated at 65°C for another 15 min (100  $\mu L$  beads for 1ml of lysate) in hybridization chamber, followed by slowly reducing the temperature to 37°C and one hour incubation. The beads were washed three times (5 min each time) in Wash Buffer 1 (50 mM Tris, pH 7.5, 0.3 M LiCl, 1% SDS, 0.5% Nonidet-P 40, 1mM DTT, 1mM PMSF, 1X protease inhibitors) at 37°C followed by treatment with 20 U of Turbo DNase I in 300  $\mu L$  of DNase I digestion buffer with the addition of 0.3 M LiCl, protease inhibitors, and superaseln at 37°C for 10 min. Then, beads were washed two more times at 37°C in the Wash Buffer1. The lysates were further washed at 37°C for 5 min in Wash Buffer 2 (1% SDS, 1mM DTT, 5mM EDTA, 150mM NaCl, 1mM PMSF). Proteins were eluted in 600  $\mu L$  of Elution Buffer (10 mM Tris, pH 7.5, 1 mM EDTA) at 70°C for 5 min. DNA probes for iDRiP were ordered from Integrated DNA Technologies and labeled with 3' biotin-TEG.

#### Detection of TERC-TERRA interaction from UV-crosslinked cells

TERRA RNA capture were performed using the iDRiP protocol described above. After elution, RNA was extracted using TRIzol and cDNA was synthesized using random primers.

#### Quantitative proteomics

Proteins enriched with each lncRNA were suspended in 4 M urea/50 mM HEPES (pH 8.5). As described previously (Edwards and Haas, 2016), disulfide bonds were reduced, free thiols were alkylated with iodoacetamide; proteins were purified by MeOH/ $CHCl_3$  precipitation and digested with Lys-C and trypsin, and peptides were labeled with TMT-10plex reagents (Thermo Scientific) (McAlister et al., 2012). Labeled peptide mixtures were pooled into two 10-plexed samples, which were fractionated by basic reversed-phase HPLC as described previously (Edwards and Haas, 2016). Twelve fractions were analyzed by multiplexed quantitative proteomics performed on an Orbitrap Fusion mass spectrometer (Thermo Scientific) using a Simultaneous Precursor Selection (SPS) based MS3 method (McAlister et al., 2014). MS2 spectra were assigned using a SEQUEST-based (Eng et al., 1994) proteomics analysis platform (Huttlin et al., 2010). Peptide and protein assignments were filtered to a false discovery rate of < 1% employing the target-decoy database search strategy (Elias and Gygi, 2007) and using linear discriminant analysis and posterior error histogram sorting (Huttlin et al., 2010). Peptides with sequences contained in more than one protein sequence from the UniProt database were assigned to the protein with most matching peptides (Huttlin et al., 2010). We extracted TMT reporter ion intensities as those of the most intense ions within a 0.03 Th window around the predicted reporter ion intensities in the collected MS3 spectra. Only MS3 with an average signal-to-noise value of larger than 20 per reporter ion as well as with an isolation specificity (Ting et al., 2011) of larger than 0.75 were considered for quantification. A two-step normalization of the protein TMT-intensities was performed by first normalizing the protein intensities over all acquired TMT channels for each protein based on the median average protein intensity calculated for all proteins. To correct for slight mixing errors of the peptide mixture from each sample a median of the normalized intensities was calculated from all protein intensities in each TMT channel and the protein intensities were normalized to the median value of these median intensities.

#### Proteomics network and GO analysis

To visualize potential reciprocal and intertwined interactions among the TERRA proteome, data from iDRiP-MS biological replicates was analyzed and the network was generated through the use of QIAGEN's Ingenuity Pathway Analysis (IPA, QIAGEN Redwood City, <https://www.qiagenbioinformatics.com>). Gene ontology (GO) term was analyzed by DAVID Bioinformatics Resources 6.7 (<https://david.ncifcrf.gov/>) (Huang et al., 2009a)

#### Immuno-FISH

Cells were cytospun, CSKT treated (10 mM PIPES, pH 6.8, 100 mM NaCl, 3 mM  $MgCl_2$ , 0.3 M sucrose, 0.5% Triton X-100, adjust to pH 6.8), and fixed in 4% paraformaldehyde and stored at 70% EtOH at  $-20^\circ C$ . For immuno-RNA FISH, coverslips were blocked at 1% BSA/PBS with 1 mM EDTA and 0.8 U/ $\mu l$  of RNase inhibitor at 4°C for 1 hr. Cells were incubated with primary antibodies in blocking

solution at 4°C for 2 hr, and washed with 0.2% Tween20/PBS 3 times at RT. Followed by incubation of secondary antibodies (in blocking solution) at 4°C for 30 min, cells were washed with PBS 3 times and fixed in 4% paraformaldehyde for 10 min. RNA FISH was then performed as described previously. Antibodies were used against ATRX (Cat#: sc-15408, Santa Cruz), TRF2 (Cat#: sc-9143, Santa Cruz) and RAP1 (Cat#: sc-28197, Santa Cruz). For immuno-telomeric DNA FISH, cells were fixed as previously described, and were treated with RNaseA (400 µg/ml) in PBS at 37°C for 30 min. After PBS washes, slides were dehydrated by EtOH, heated to 85°C on the heating block for 5 min. PNA probes (TelC-Alexa488 or TelG-Cy3) for telomeric DNA were heated at 85°C for 5 min in hybridization buffer (20mM Tris-HCl, pH 7.5, 70% formamide, 0.1 µg/ml salmon sperm DNA), added onto preheated slides, covered by coverslips, and then incubated at 85°C in a hybridization oven for 15 min. Followed by slowly decreasing the hybridization temperature by bringing the heating block (with slides on top of it) to room temperature (RT), slides were incubated in the dark at room temperature for 2 hr. Slides were washed at 57°C (1X PBS, 0.02% Tween20) for 20 min, and washed again at RT. Slides were fixed at 4% paraformaldehyde for 5 min at RT, washed twice with PBS, incubated with blocking solution (1% BSA, PBS) at RT for 30 min, incubated with antibodies against phospho-histone H2A.X (Final Conc 1:400 dilution, Cat#05-636, clone JBW301, EMD Millipore) at 4°C overnight.

### Electrophoretic mobility shift assay (EMSA)

EMSAs and competition assays were performed as described previously (Cifuentes-Rojas et al., 2014). Short ssDNA (30 nt), dsDNA (30 bp), RNA (30 nt) and long ssDNA (80 nt) were purchased from IDT (Integrated DNA technologies). Long RNA (83 nt) was generated by in vitro transcription. Long dsDNA (80bp) was generated by T4 DNA polymerase filling method using the same templates as in vitro transcription, and filling in DNA by adding T4 DNA polymerase and T7 oligos at 37°C for 15 min. All probes were PAGE-purified.

### RQ-TRAP and TRAP assays

RQ-TRAP was performed and quantified as described in (Cristofari and Lingner, 2006) with minor modifications. Reactions were performed with iTaq Universal SYBR Green Supermix (Bio-Rad) supplemented with 0.5 mM MgCl<sub>2</sub>. Heat-inactivated cell extract (10 min, 95°C) was used as negative control for telomerase activity. TRAP assay was performed in parallel to validate the results seen by RQ-TRAP. TRAP was performed as described in (Chen et al., 2013). Briefly, undiluted (28 ng) and serial dilution of cell extracts in Chaps buffer were incubated at 30°C for 30 min. The 50 µL reactions contained: 1x TRAP buffer (20 mM Tris-HCl pH 8.3, 6.5 mM MgCl<sub>2</sub>, 63 mM KCl, 0.005% Tween-20, 1 mM EGTA, 0.1 mg/ml BSA), 25 µM dNTPS, 2 ng primer TS, 4 µCi dGTP[α-<sup>32</sup>P] (stock: 6000Ci/mmol). Following heat-inactivation at 94°C for 1 min, 2U Taq polymerase and 2 ng primer ACX was added for 27 PCR cycles (30 s at 94°C and 30 s at 60°C). Following PCR-amplification, 10% of the reaction was resolved on a 12% polyacrylamide gel. The gel was dried, exposed to PhosphorImager screens prior to quantification using ImageQuant (GE Healthcare LS).

### Knockdown ATRX by siRNA

Mouse ESCs were transfected with 20 nM of siRNAs using lipofectamine RNAiMAX (ThermoFisher) reagents for 48 hr in the feeders-cultured condition, and feeders were removed before harvesting ESCs. Two siRNAs (siRNA ID#s76136 and s76137, *Silencer*®Select, ThermoFisher) against ATRX and one control siRNA were used.

### Metaphase analysis of telomeric integrity

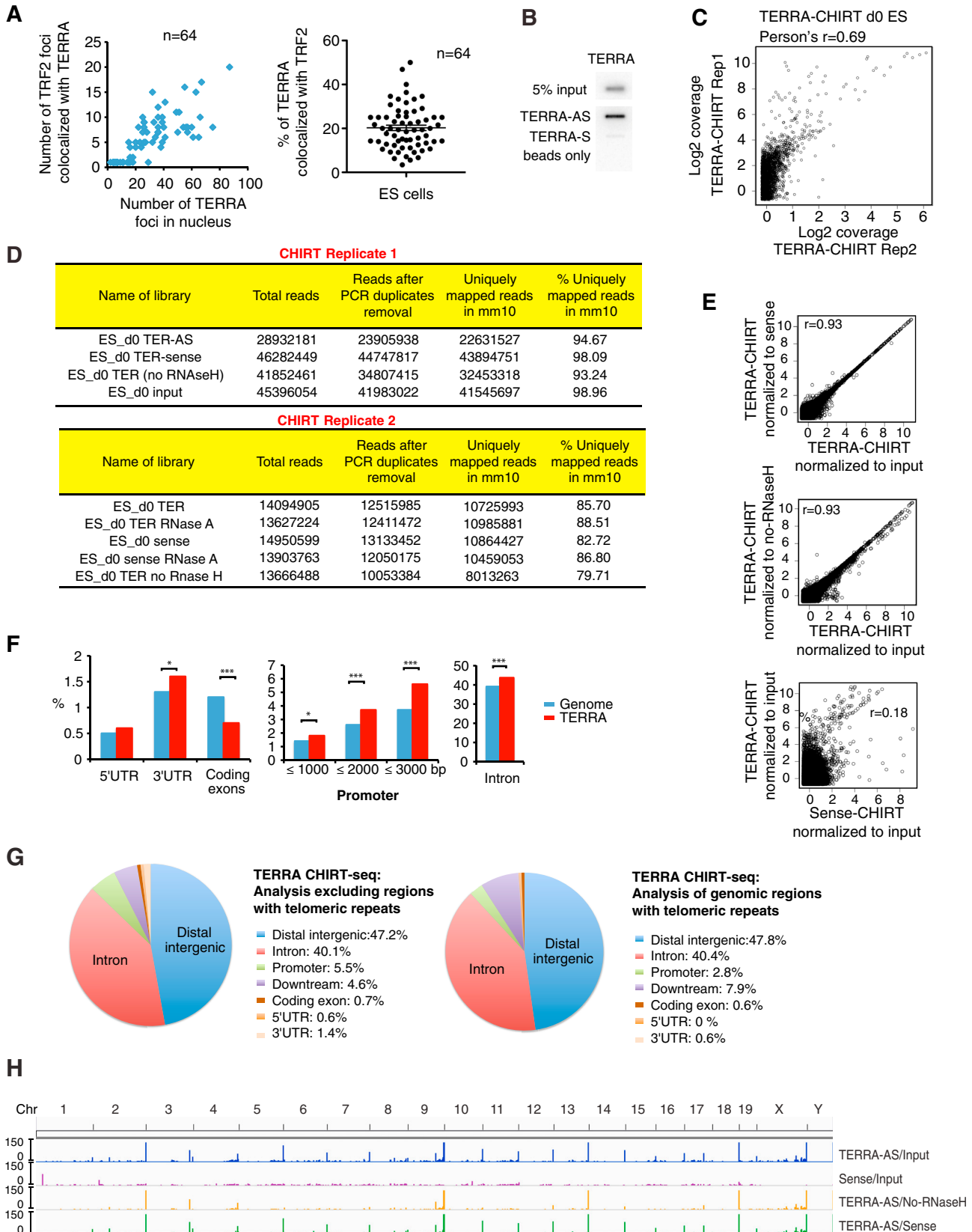
After treatment of Colcemid (1 µg/ml) for 1 hr, ESCs were collected. Followed by PBS wash, cells were incubated with 5 mL of ice-cold 0.56% KCl at RT for 6 min, and spun down at 1,000 rpm for 5 min. Cells were resuspended with 200 µL of 0.56% KCl and slowly supplied with 5 mL of ice-cold fixative (MeOH:Acetic acid::3:1, one small drop each time). Cells were spun down and transferred to 1 mL tube, and washed with 1 mL of fixative for 3 times. Cells were resuspended in fixative and ready to drop. Slides were faced down into the steam of hot water bath (80°C) and 20 µL of cells were dropped to the slide. After drying the slide for overnight, cells were fixed in 4% paraformaldehyde for 5 min at RT. After several washes with PBS, telomere DNA FISH was performed using PNA probes as described above. Loss of telomeric integrity was manifested by occurrence of multiple aberrant telomeric phenotypes on metaphase chromosomes. (i) Loss of the (TTAGGG)<sub>n</sub> telomeric repeat sequence on both sister chromatids or just on one sister chromatid (“heterogeneous”); (ii) duplications of telomeric repeats at chromosomal ends; (iii) insertions of telomeric repeats within internal chromosomal regions; and (iv) fusions between sister chromatid telomeres that would create a “ring” structure on long arm of chromosomes.

### QUANTIFICATION AND STATISTICAL ANALYSIS

Statistical parameters including the exact value of n, SD, SE, Pearson’s R correlation test, and statistical significance are reported in the figures and the figure legends. Statistical significance is determined by the value of  $p < 0.05$  by two-tailed Student’s t test or Fisher exact test, or Chi-square test, where appropriate.

### DATA AND SOFTWARE AVAILABILITY

Raw data and processed files for the TERRA-CHIIRT and RNA sequencing have been deposited in the NCBI Gene Expression Omnibus database under accession number GEO: GSE79180.



---

**Figure S1. TERRA CHIRT-Seq Statistics, Related to Figure 1**

(A) TERRA colocalization counts with TRF2 for the data in Figure 1C. 414 out of 2014 TERRA foci (19.7%) were colocalized with TRF2 in mouse ESCs. n = number of counted nuclei.

(B) RNA slotblot analysis showing that TERRA-AS specifically captured TERRA RNA by CHIRT. Total RNA was extracted from beads after probe hybridization without RNase H elution.

(C) Scatterplot comparing Log2 coverages of biological replicates for TERRA CHIRT-seq analysis in ESCs. Pearson's r was shown. Replicate 1 (Rep1) was normalized with input. Replicate 2 (Rep2) was normalized to RNaseA pre-treated control.

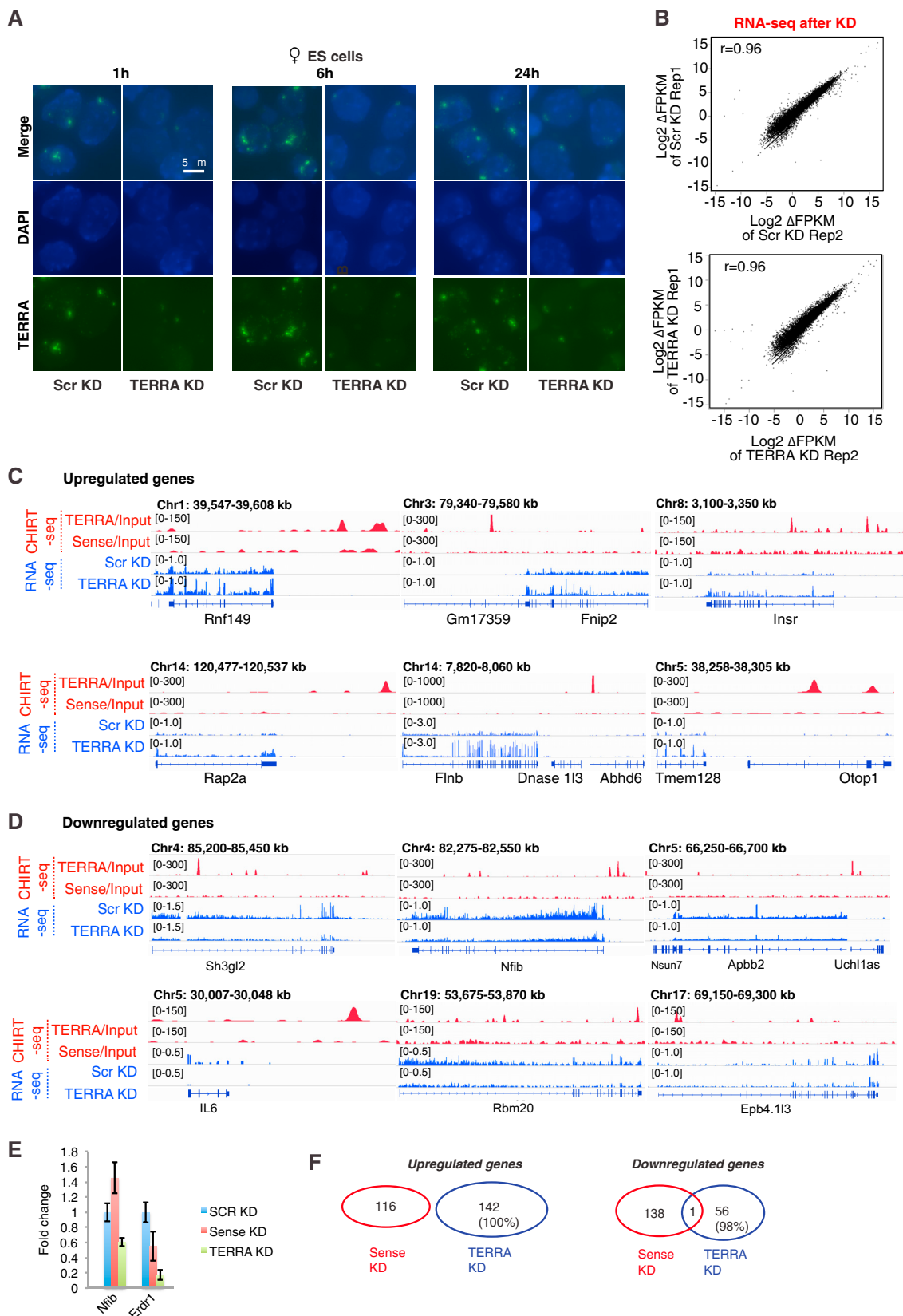
(D) Read statistics for two biological replicates of the TERRA CHIRT-seq analysis.

(E) Scatterplot analysis comparing log2 coverages of TERRA CHIRT normalized using different methods. Pearson's r shown.

(F) CEAS analysis shows significant over-representation of introns and noncoding regulatory regions. Exons are under-represented. \*\*\*p < 0.001; \*p < 0.05 (one-sided binomial test). The genome reference was obtained from the CHIRT input.

(G) CEAS analysis: Left panel, Pie chart showing relative representation of various genomic regions when the CHIRT analysis excludes genomic regions containing telomeric repeats. Right panel, Pie chart showing relative representation of various genomic regions when the CHIRT analysis is performed on genomic regions containing telomeric repeats.

(H) CHIRT-seq tracks showing TERRA enrichment at the ends of various chromosomes in female ESCs. Different normalization methods reveal similar results (TERRA/input; TERRA/no RNase H; TERRA/sense). Note: TERRA-Sense CHIRT did not resemble TERRA-AS CHIRT.



(legend on next page)

---

**Figure S2. RNA-Seq Analysis after TERRA Knockdown by LNA Gapmers, Related to Figure 2**

(A) RNA FISH confirming TERRA depletion after 1, 6, and 24 hr of LNA treatment in ESCs.

(B) Scatterplots comparing log<sub>2</sub> FPKM values show good correlation between biological replicates of RNA-seq in both Scr KD and TERRA KD in ESCs. Pearson's  $r$  is shown.

(C) CHIRT-seq tracks (red) for TERRA binding sites near differentially upregulated genes after TERRA KD in ESCs. RNA-seq coverage is FPM (fragments per million)-normalized and tracks are shown in blue.

(D) CHIRT-seq tracks (red) for TERRA binding sites near differentially downregulated genes after TERRA KD in ESCs. RNA-seq coverage is FPM (fragments per million)-normalized and tracks are shown in blue.

(E) Quantitative RT-qPCR of *Nfib* and *Erd1* expression after Scr, sense, or TERRA LNA knockdown.

(F) RNA-seq analysis of sense LNA knockdown controls show largely non-overlapping changes in comparison to TERRA-specific knockdown.

**A Downregulated genes**

GO Term	Count	P-Value	Benjamini
TOR signaling	3	1.1E-3	3.6E-1
cellular response to corticotropin-releasing hormone stimulus	2	1.1E-2	8.9E-1
protein localization	3	1.1E-2	7.8E-1
positive regulation of transcription from RNA polymerase II promoter	7	1.6E-2	8.1E-1
negative regulation of transcription from RNA polymerase II promoter	6	1.6E-2	7.4E-1
negative regulation of hormone secretion	2	2.1E-2	7.7E-1
negative regulation of pri-miRNA transcription from RNA polymerase II promoter	2	2.1E-2	7.7E-1
post-embryonic development	3	2.4E-2	7.6E-1
negative regulation of cAMP-dependent protein kinase activity	2	3.1E-2	8.1E-1
neuron maturation	2	3.1E-2	8.1E-1
clathrin coat assembly	2	3.1E-2	8.1E-1

**B Upregulated genes**

GO Term	Count	P-Value	Benjamini
heart development	10	5.8E-5	4.5E-2
protein phosphorylation	12	1.5E-3	4.5E-1
positive regulation of telomere capping	3	4.9E-3	7.3E-1
organ morphogenesis	5	5.8E-3	6.9E-1
negative regulation of MAPK cascade	3	6.8E-3	6.7E-1
regulation of JNK cascade	3	6.8E-3	6.7E-1
protein glycosylation	5	7.3E-3	6.2E-1
protein ADP-ribosylation	3	7.6E-3	5.8E-1
transcription elongation from RNA polymerase II promoter	3	9.1E-3	6.0E-1
response to calcium ion	4	1.0E-2	6.0E-1

**C Upregulated genes\_Telomerase pathway**

GENE NAME
epidermal growth factor receptor(Egfr)
insulin-like growth factor I receptor(Igf1r)
tankyrase, TRF1-interacting ankyrin-related ADP-ribose polymerase(Tnks)

**Figure S3. GO Analysis of Upregulated and Downregulated Genes following TERRA Depletion, Related to Figure 2**  
 Enriched pathways are identified by DAVID bioinformatics resources. p values determined by Fisher Exact test. Benjamini FDR shown.

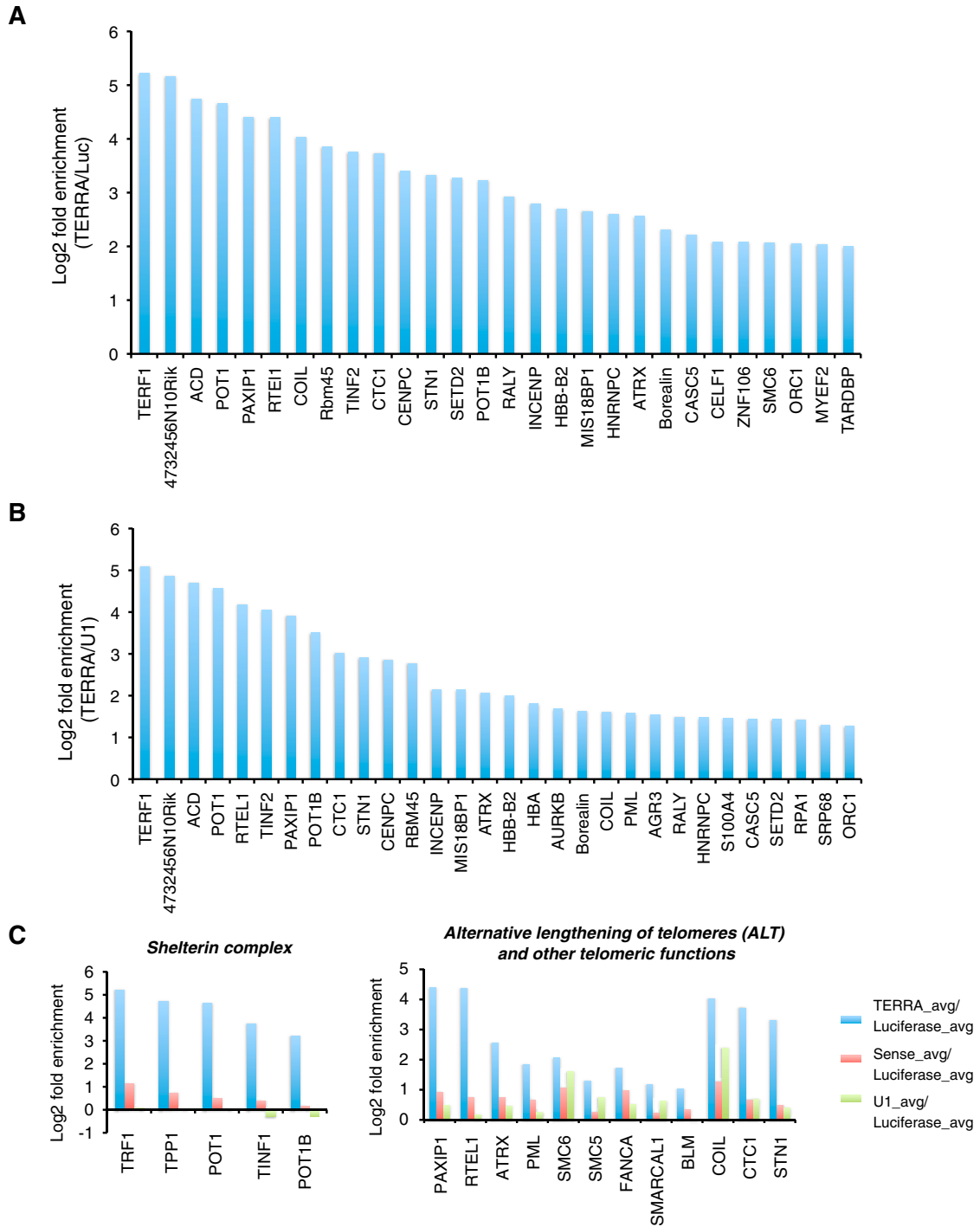


**Figure S4. TERRA iDRiP Proteomics, Related to Figure 3**

(A) Top 30 candidates of TERRA iDRiP proteomics with the highest enrichment over the luciferase RNA capture are shown.

(B) Top 30 candidates of TERRA iDRiP proteomics with the highest enrichment over the U1 RNA capture are shown.

(C) Shelterin complex and telomere function associated proteins are enriched in TERRA iDRiP proteomics but not in the sense-probe or the U1 RNA proteomics. The intensities of indicated proteins were normalized to luciferase RNA iDRiP proteomics. Log2 fold enrichment was shown as the y axis.

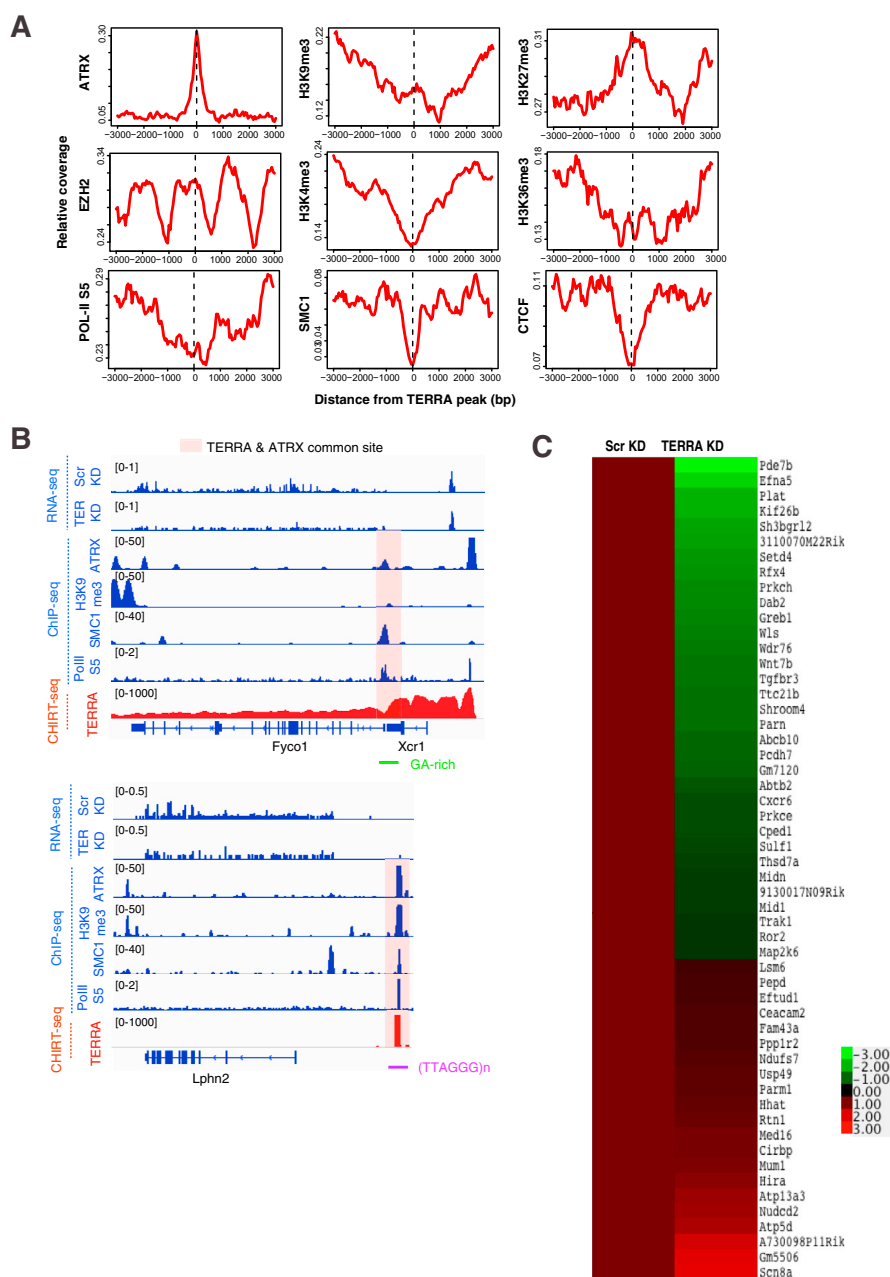


**Figure S5. Gene Expression of ATRX-TERRA Target Genes after TERRA KD, Related to Figure 4**

(A) Metasite analysis as described in Figure 4A but with telomere-bound TERRA peaks subtracted from analysis. ChIP-seq coverage of indicated epitopes (y axis) relative to averaged TERRA-binding site (x = 0).

(B) TERRA depletion results in *Lphn2* and *Fyco1* downregulation. Genome browser shot of two examples of TERRA targets, with RNA-seq, ChIRT-seq, and ChIP-seq data displayed.

(C) Heatmap shows the downregulation genes (green,  $\log_2 < 0.5$  of delta FPKM) and the upregulation (red,  $\log_2 > 0.5$  of delta FPKM) genes for ATRX/TERRA target after TERRA depletion.

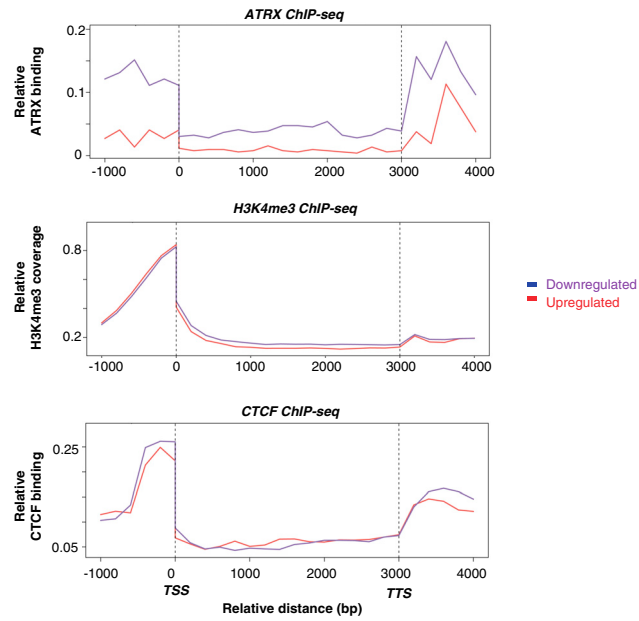


**Figure S6. ATRX Is Enriched near the TSS of Genes Sensitive to TERRA Depletion, Related to Figure 4K**

Relationship of ATRX, H3K4me3, and CTCF coverage profiles shown in metagene plots for genes that are upregulated (red) or downregulated (blue) after TERRA depletion. Note that ATRX coverage is enriched near the TSS of genes that are downregulated when TERRA is depleted. This trend was not observed for other epitopes, including H3K4me3 and CTCF.

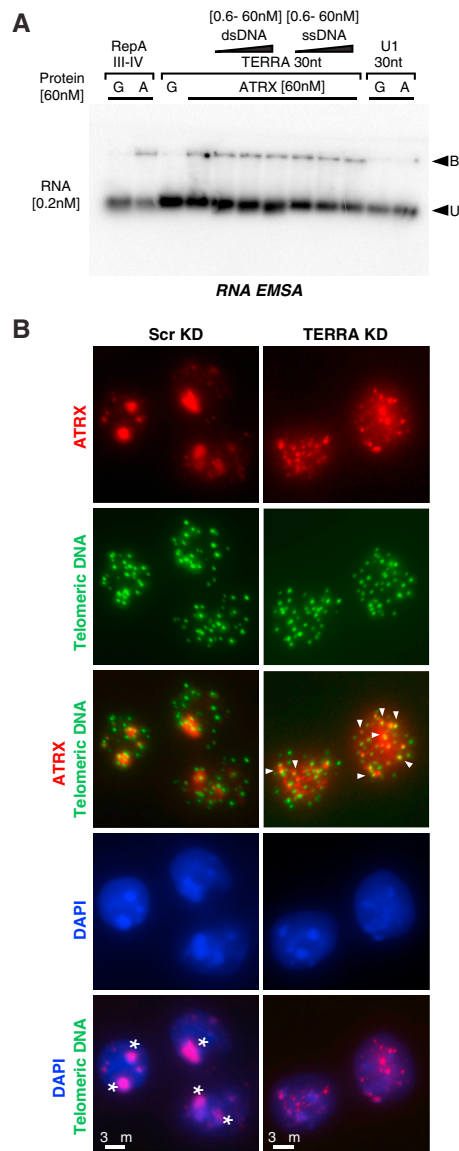


**Figure S7. TERRA-ATRX Interactions Are Not Competed Away by DNA, Related to Figure 5**

(A) Competition assay: TERRA RNA shifted by ATRX cannot be competed away by increasing concentrations (0.6, 6, 60nM) of dsDNA (30bp) or ssDNA (30nt) of corresponding TERRA sequence (30nt). RNA EMSA with 0.2 nM RNA probes from indicated transcripts (top) and 60nM GST (G, control) or ATRX (A) protein. Bound probe (shifted), B. Unbound, U.

(B) Additional examples of TERRA depletion (6hr knockdown) causing ATRX dispersal from pericentric heterochromatin and relocalization to telomeres in ESCs. Immuno-DNA-FISH staining for ATRX and telomeric DNA reveals large ATRX foci (red) on pericentric heterochromatin (dense DAPI staining) in control cells. TERRA depletion cells show dispersed ATRX signals that coincide with telomeric DNA (green). Asterisks are ATRX foci at pericentric heterochromatin. Arrowheads are ATRX foci at telomeres.